Zeitschrift: Schweizerische mineralogische und petrographische Mitteilungen = Bulletin suisse de minéralogie et pétrographie

Band: 78 (1998)

Heft: 1

Vereinsnachrichten: Bericht über die 72. Hauptversammlung der Schweizerischen Mineralogischen und Petrographischen Gesellschaft in La Chaux-de-Fonds : 9./10. Oktober 1997

Nutzungsbedingungen

Die ETH-Bibliothek ist die Anbieterin der digitalisierten Zeitschriften auf E-Periodica. Sie besitzt keine Urheberrechte an den Zeitschriften und ist nicht verantwortlich für deren Inhalte. Die Rechte liegen in der Regel bei den Herausgebern beziehungsweise den externen Rechteinhabern. Das Veröffentlichen von Bildern in Print- und Online-Publikationen sowie auf Social Media-Kanälen oder Webseiten ist nur mit vorheriger Genehmigung der Rechteinhaber erlaubt. Mehr erfahren

Conditions d'utilisation

L'ETH Library est le fournisseur des revues numérisées. Elle ne détient aucun droit d'auteur sur les revues et n'est pas responsable de leur contenu. En règle générale, les droits sont détenus par les éditeurs ou les détenteurs de droits externes. La reproduction d'images dans des publications imprimées ou en ligne ainsi que sur des canaux de médias sociaux ou des sites web n'est autorisée qu'avec l'accord préalable des détenteurs des droits. En savoir plus

Terms of use

The ETH Library is the provider of the digitised journals. It does not own any copyrights to the journals and is not responsible for their content. The rights usually lie with the publishers or the external rights holders. Publishing images in print and online publications, as well as on social media channels or websites, is only permitted with the prior consent of the rights holders. Find out more

Download PDF: 16.01.2026

ETH-Bibliothek Zürich, E-Periodica, https://www.e-periodica.ch

SCHWEIZ. MINERAL. PETROGR. MITT. 78, 185–220, 1998

Bericht über die 72. Hauptversammlung der Schweizerischen Mineralogischen und Petrographischen Gesellschaft in La Chaux-de-Fonds

9./10. Oktober 1997

72. annual meeting of the Swiss Society of Mineralogy and Petrology at La Chaux-de-Fonds

October 9–10, 1997

Zusammenfassungen der Vorträge und Poster

Abstracts of oral communications and posters

MINERLAOGY 185
PETROLOGY: THEORETICAL/EXPERIMENTAL 190
PETROLOGY: MAGMATIC, VOLCANIC 193
METAMORPHIC PETROLOGY 199
GEOCHRONOLOGY AND GEOCHEMISTRY 205
ORE DEPOSITS 211
APPLIED MINERALOGY AND PETROLOGY 213
ANALYTICAL METHODS 217

MINERALOGY

P. Berlepsch and R. Miletich (Basel, Bayreuth):

K <–> Tl substitution in hydrothermally synthesized (Tl,K)Sb_5S_8 parapierrotites.

The geochemical affinity between thallium (Tl) and potassium (K), which results from the practically identical effective ionic radii, is responsible for the abundance of thallium in rock-forming minerals (ZEMANN, 1993; CERNY et al., 1985). Significant substitutions has been reported in particular for oxygen-based mineral phases, e.g. dorallcharite (BALIĆ-ŽUNIĆ et al., 1994) or perlialite (ARTIOLI and KVICK, 1990). However, this substitution can be observed in sulfides as well. Significant substitutions of thallium by alkali-metals in such minerals are reported e.g. for chalcothallite (SEMENOV et al., 1967), galkhaite (GRUZDEV, 1972), or rohaite (KARUP-MØLLER, 1978).

We report the K <–> Tl substitution for the parapierrotite-type MSb_5S_8 (M = Tl, K) structure. Both synthetic end-member and solid solutions were obtained from strongly alkaline (pH > 10) hydrothermal solutions at temperatures between 200 and 230 °C. In order to achieve crystal growth under hydrothermal conditions, $Tl(I)NO_3$, S, and $Sb(III)_2O_3$ were used as starting materials and reacted with MOH (M = Na, K) aqueous solutions in polytetrafluoroethylen-lined autoclaves. Euhe-

dral crystal up to 1 mm in size were obtained by cooling with rates of less than 1°/min. Microprobe analyses showed the $(K,Tl)Sb_5S_8$ crystals to be free of significant amounts of sodium. The determination of the crystal structure of Tl-free end-member KSb_5S_8, a = 8.1374(5), b = 19.5013(5), c = 9.0612(5) Å, β = 91.932(5)°, V = 1437.23(12) Å^3, by single-crystal X-ray diffraction confirmed Pn space-group symmetry and isostructural atomic arrangement as in aristotype parapierrotite (ENGEL, 1980; JOHANN et al., 1975). Details of the structural investigations of both end-member and solid solution compositions, the crystal chemistry and cation ordering of $(Tl,K)Sb_5S_8$ parapierrotites will be discussed.

ARTIOLI, G. and KVICK, A. (1990): Synchrotron X-ray Rietveld study of perlialtite, the natural counterpart of synthetic zeolite-L. Eur. J. Mineral., 2, 749–759.

BALIĆ-ŽUNIĆ, T., MOËLO, Y., LONCAR, Z. and MICHEELSEN, H. (1994): Dorallcharite, $Tl_{0.8}K_{0.2}Fe_3(SO_4)_2(OH)_6$, a new member of the jarosite-alunite family. Eur. J. Mineral., 6, 255–263.

CERNY, P., MEINTZER, R.E. and ANDERSON, A.J. (1985): Extreme fractionation in rare-element granitic pegmatites – selected examples of data and mechanisms. Canad. Mineralogist, 23, 381–421.

ENGEL, P. (1980): Die Kristallstruktur von synthetischem Parapierrotit, $TlSb_5S_8$. Z. Krist., 151, 203–216.

GRUZDEV, V. (1972): Galkhaite ($HgAsS_2$), a new mineral from arsenic-antimony-mercury deposits of the USSR. Dokl. Akad. Nauk SSSR, 205, 1194–1197 (in Russian).

JOHANN, Z., PICOT, P., HAK, J. and KVACEK, M. (1975): La parapierrotite, un nouveau minéral thallifère d'Allchar (Yougoslavie). Tscherm. mineral. petrogr. Mitt., 22, 200–210.

KARUP-MØLLER, S. (1978): The ore minerals of the Ilimaussaq intrusion: their mode of occurrence and their conditions of formation. Grønl. Geol. Unders., 127, 1–51.

SEMENOV, E.I., SØRENSEN, H., BESSMERTNAYA, M.S. and NOVOROSSOVA, L.E. (1967): Chalcothallite, a new sulphide of copper and thallium from the Ilimaussaq intrusion, South Greenland. Medd. Grønland, 5, 13–26.

ZEMANN, J. (1993): Thallium in Mineralogie und Geochemie. Mitt. Österr. Mineral. Ges., 138, 75–91.

G.G. Biino (Berkley, Fribourg):

Quantitative description of mineral surface phenomena.

Any quantitative description of mineral surface phenomena implies the characterization of atomic identities, atomic position, bond length, and bond directions whithin 3 to 5 atomic monolayers. We have studied the time dependence of the oxidation of the W(110) surface via chemical-state-resolved photoelectron spectroscopy and diffraction (YNZUNZA et al., 1997). The well characterized W(110) system was used as a reference case to check the accuracy of structure determinations from photoelectron diffraction. The experimental run at the Advanced Light Source lasted 70 minutes (with a traditional source, a comparable high-resolution data set is prohibitely time consuming to obtain). Data obtained over nearly the full 2 π solid angle above the surface. We experimentally proved the decay and growth of various chemical state specific peaks in the W $4f_{7/2}$ spectra, i.e.: the bulk peak, the clean surface peak at 320 meV lower binding energy, a peak associated with W atoms bound to two oxygen atoms at a 350 meV higher binding energy and a peak associated with W atoms bound to three oxygen atoms at a 730 meV higher binding. We can quantify conclusions concerning the reaction kinetics involved. We have also measured the full-solid-angle photoelectron diffraction patterns for the two oxygen induced W states, and comparing these with photoelectron diffraction calculations we obtain the local atomic positions of the two different types of oxygen atoms on the surface. We have also reproduced the same experiment but the detection was done with Low Energy Electron Diffraction (LEED) patterns were collected at regular time laps for 28 hours, but the oxidation of the W(110) surface was not evidenced. The monitoring of the oxidation can be done with a short range probe such as photoelectron diffraction, but can not be done with LEED due to its necessity of long range order. Being able to simultaneously use photoelectron diffraction to determine local geometries around species with different chemical states represents a unique capability that should be broadly applicable to various surface reactions, epitaxial growth processes and mineralogy. Biino and coworkers have thus applied X-ray photoelectron spectroscopy (XPS) and diffraction (XPD) to phyllosilicates which control key sorption/desorption processes in the upper part of the Earth's crust. The element-specific nature of XPD permits studying the short-range atomic structure around Al and thus identifying their local chemical environment, something which has not been possible via traditional X-ray diffraction analyses (which are not element specific). In particular, we will consider the degree of Al order in the tetrahedral sites of mica, and present experimental XPD data together with multiple scattering simulations for different structures.

YNZUNZA, R.X., BIINO, G.G., PALOMARES, F.J., TOBER, E.D., WANG, Z., MORAIS, J., DENECKE, R., LIESEGANG, J., HUSSAIN, Z., VAN HOVE, M.A and FADLEY, C.S. (1997): Study of the oxidation of W(110) with chemical state- and time-resolved photoelectron spectroscopy and diffraction. AVS97.

C. Ferraris (Fribourg):

Polytypism and polysomatisme in some Alpine micas: HRTM / AEM data.

High Resolution Transmission Electron Microscopy (HRTEM) allows to image mica structures with a spatial resolution from 3 to 1 Å. By a combination of this technique with Analytical Electron Microscopy (AEM) it is possible to obtain data on mineral transformation at the nano scale. Several samples of magmatic and metamorphic micas have been characterised by their polytype periodicity. Polytypic phenomena have been studied by SAED (Selected Area Electron Diffraction) and HRTEM images obtained from samples cut across the (001) layers. Sequences of different polytype blocks which are few layers thick and coherently intergrown along [001] have been identified.

Looking across the layers reveals, in some samples, a succession of polytype blocks 1M, $2M_1$ and 3T, and sometimes a semi random 1 Mrn (120) basic structure. The latter gives almost continuous streaks along hkl diffraction rows with $k \neq 3$ n but, sometimes, intensity modulations appear along such streaks; they indicate either significant amounts of short range ordering in such semi randomness zone (BARONNET et al., 1993). Alternating slabs of each polytype blocks are a few layers thick but of varying thickness. The transition zones between two ordered blocks or between an ordered and a semi random one are characterised by the presence of stacking faults; a common feature is that they correspond to layer displacement faults, this means that in the normal polytype blocks (1M, $2M_1$, 3T and 1Mrn [120]) a single layer is shifted from its normal position.

In some cases the complex local microstructure of micas is shown. Several types of layer can coexist in a single grain (polysomatism). Interstratification of mixed layers has been resolved by comparing the different thickness of the layer stacking sequence and using AEM when possible. Typical interlayering was observed in samples of mica/chlorite and mica/serpentine

BARONNET, A., NITSCHE, S. and KANG, Z.C. (1993): Layer stacking microstructures in a biotite single crystal. A combined HREM-AEM study. Phase Transition, 43, 107–128.

Th. Kohler, Th. Armbruster and E. Libowitzky (Bern, Pasadena):

Hydrogen bonding and Jahn-Teller distortion in groutite, α-MnOOH, and manganite, γ-MnOOH, and their relations to ramsdellite, MnO_2, and pyrolusite, β-MnO_2. (Poster)

Since the most recent studies on groutite (GLASSER et al., 1968) and manganite (DACHS, 1963), X-ray data acquisition and correction procedures have become significantly improved. In addition, structures of twinned crystals can be refined from single-crystal data. Thus, it was an aim of this contribution to locate hydrogen atoms even in these transition metal oxyhydroxides with X-ray methods. The relatively short O–H···O distances (ca. 2.6 Å) in MnOOH polymorphs give rise to characteristic IR absorptions which are not well understood as yet. Thus, oriented single-crystal IR absorption spectra were collected and interpreted. Furthermore, temperature dependent cell dimensions as well as topotactic relations between MnOOH and MnO_2 polymorphs were investigated by in situ high temperature X-ray diffraction studies of groutite and manganite under oxidizing conditions.

The crystal structure of α-MnOOH, groutite (space group *Pnma*, $a = 10.667(1)$, $b = 2.871(1)$, $c = 4.554(1)$ Å, $Z = 4$) and manganite, γ-MnOOH (space group $P2_1/c$, $a = 5.304(1)$, $b = 5.277(1)$, $c = 5.304$ Å, $\beta = 114.38(2)°$, $Z = 4$), both from the Kalahari manganese field (South Africa), were refined including hydrogen positions from room temperature X-ray single-crystal data. The refinements converged to R-values of 1.5% for 479 (groutite) and to 2.0% for 821 (manganite) unique reflections, respectively. A (101) twin refinement based on F^2_{obs} was applied for manganite leading to a twin contribution of ca. 0.9 : 0.1. The structures of groutite and manganite are distorted derivatives of the MnO_2 polymorphs ramsdellite and pyrolusite (rutile structure), respectively. The structural distortions of the oxyhydroxides are caused by an interaction of Jahn-Teller distortion of octahedrally coordinated Mn^{3+} (four short and two long Mn–O distances) and hydrogen bonding. In both structures two symmetrically distinct O sites (O1 and O2) are three-coordinated by Mn^{3+}. The choice which O site forms an OH group is governed by the orientation of the Jahn-Teller distortion and space constraints dictated by the octahedral framework topology. The two long Mn–O bonds are formed by both O1 and O2 thus the Jahn-Teller distortion alone does not determine the preference of the OH group. In groutite, the OMn_3 coordination fragment which shows the strongest deviation from planarity towards a trigonal pyramid bonds to H where the O–H vector points perpendicular to the Mn_3 plane. In manganite the coordinations of O1 and O2 are very similar, thus H shows longe range dis-

order as observed by twinning. Both, groutite and manganite have short O–H···O distances (2.6 Å) giving rise to peculiar IR absorption features between 3200 and 1800 cm^{-1}. Oriented single-crystal slabs of manganite and diaspore (isostructural to groutite) were studied by polarized FTIR spectroscopy at 82 and 298 K and all H-bonding related IR-absorptions were assigned. Manganite, γ-MnOOH, and groutite, α-MnOOH both transform in air above ca. 300 °C to β-MnO_2 (pyrolusite) which was studied by in situ temperature dependent single-crystal X-ray diffraction. The topotactic relation is preserved during the transformation.

GLASSER, D.L.S. and INGRAM, L. (1968): Refinement and structure of groutite, α-MnOOH. Acta Cryst. B24, 1233–1236.

DACHS, H. (1963): Neutronen- und Röntgenuntersuchungen am Manganit, MnOOH. Z. Krist. 118, 303–326.

P. Berlepsch, Th. Armbruster, J. Brugger, E.Y. Bykova and P.M. Kartashov (Basel, Bern, Victoria, Moskau):

The crystal structure of natural $Cu_3O[SO_4(Mo,S)O_4]$ and its relation to synthetic $Cu_3O[MoO_4]_2$. (Poster)

The crystal structure of the natural compound, $Cu_3O[SO_4(Mo,S)O_4]$, from the Large Tolbachik Fissure Eruption (1975–1976) on Kamchatka peninsula (Russia) was determined from single-crystal X-ray data (space group *Pnma*, Z = 4, a = 7.421(2), b = 6.754(3), c = 13.624(5) Å) and refined to $R1$ = 3.95%. The natural compound is isostructural with synthetic $Cu_3O[MoO_4]_2$ but exhibits a highly unusual substitution of S^{6+} (ionic radius 0.12 Å) for Mo^{6+} (ionic radius 0.41 Å) in tetrahedral coordination. The synthetic and the natural structures are both characterized by edge-sharing zigzag strings of Jahn-Teller distorted Cu^{2+} octahedra with attached Cu^{2+} in five-fold pyramidal coordination (4+1). The strongly distorted Cu ribbons are connected by S^{6+} and Mo^{6+} bearing tetrahedra to form a three-dimensional framework. It is assumed that the structural strain due to the unusual S^{6+} <–> Mo^{6+} substitution is balanced by development of a different type of Jahn-Teller distortion compared to the synthetic end-member variety. The substitutional disorder of S and Mo in the mineral structure leads to strong static disorder in the entire structure as revealed by relatively high atomic displacement parameters for all atoms. It is suggested that an end-member of the type $Cu_3O[SO_4]_2$ is not stable due to the restricted flexibility of the square pyramidal coordination of Cu^{2+}.

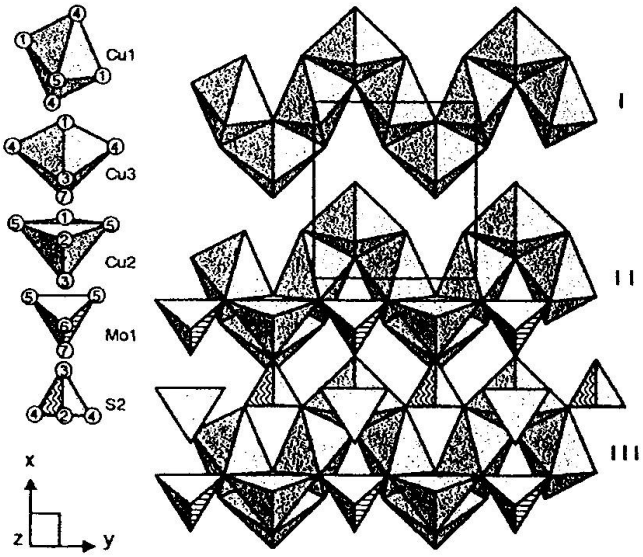

The figure shows a polyhedral model of the structure of Cu_3O $[SO_4(Mo,S)O_4]$ projected along the c-axis. Jahn-Teller distorted Cu^{2+} octahedra formed edge-sharing zizgzag ribbons along b (I). These ribbons are linked along a by (1) S2 tetrahedra corner-sharing with Cu2 square pyramids and (2) by Cu3 octahedra corner-sharing with Mo1 tetrahedra (II). A three-dimensional network is formed by bonds of the SO_4 and $(Mo,S)O_4$ tetrahedra to the neighbouring zigzag ribbons along c (III).

Th. Armbruster, J. Birrer, E. Libowitzky and A. Beran (Bern, Wien):

Crystal chemistry of Ti-bearing andradites. (Poster)

Ti-bearing andradites (space group $Ia\bar{3}d$) were investigated by single-crystal and powder X-ray diffraction methods, IR spectroscopy, optical microscopy and electron microprobe analyses. X-ray site population refinements and IR spectroscopy indicate that three of the structurally investigated crystals (two from Kaiserstuhl, Germany and one from Atlas mountains, Morocco) are andradites characterized by the schorlomite substitution $Ti^{4+} \rightarrow Si^{4+}$, where Ti^{4+} preferentially occupies the octahedral site and mainly Fe^{3+} occupies the tetrahedral vacancies. These garnets show only a very low hydrogarnet substitution of the type $O_4H_4 \rightarrow SiO_4$ giving rise to weak IR absorptions between 3400 and 3700 cm^{-1}. Ti-bearing andradites e.g., from the Zermatt area (Valais, Switzerland) and from San Benito Co. (Ca, USA) have the octahe-

dral morimotoite substitution $Fe^{2+} + Ti^{4+} \rightarrow 2\ Fe^{3+}$ coupled with a strong hydrogarnet substitution ($O_4H_4 \rightarrow SiO_4$) affecting the tetrahedral site. Comparison of electron microprobe analyses with site population refinements (X-ray data) indicates that in all analyzed Ti-bearing andradites Al is concentrated on the octahedral site. The increased cell dimension found for all Ti-bearing andradites compared to end-member andradite is explained by repulsion between Ca (dodecahedron) and Ti^{4+} (octahedron) decreasing the shared octahedral-dodecahedral edge and increasing the shared tetrahedral-dodecahedral edge. This leads to an expansion of the tetrahedron thus structural strain is released by incorporation of large cations on the tetrahedral site. Depending on the geochemical environment, oxygen fugacity, and p,T conditions either the hydrogarnet ($O_4H_4 \rightarrow SiO_4$) substitution operates or tetrahedral Fe^{3+}, Fe^{2+} substitutes for Si^{4+}. If the schorlomite substitution dominates the garnets show a dull luster and are opaque in thin sections. If a combination of the hydrogarnet and the morimotoite substitution dominates the Ti-bearing garnets often have a sparkling glassy luster and are in thin sections light to dark brown, frequently zoned, and often birefringent.

J. Stolz and Th. Armbruster (Bern):

Mg^{2+}, Mn^{2+}, Cd^{2+} and Sr^{2+} exchange in heulandite single-crystals: X-ray structure refinements. (Poster)

The crystal structure of heulandite, $(Na,K)Ca_4[Al_9Si_{27}O_{72}] \cdot 24\ H_2O$, exhibits three types of structural channels running parallel to (010). The A channel is confined by a ten-, the B and C channels by eight-membered rings of tetrahedra with a highly disordered Si,Al distribution. We took advantage of the excellent ion-exchange capability of these channels to incorporate divalent cations of different ionic radius and studied their structural arrangements. Single-crystals (0.1–0.5 mm) of a natural heulandite from Nasik, India, were placed in a teflon autoclave filled with 2M NaCl for 9 weeks at 423 K yielding a fully Na-exchanged heulandite as a precursor phase. Mg^{2+}-, Mn^{2+}-, Cd^{2+}- and Sr^{2+}-exchanged heulandites were obtained by further treatment (6–13 weeks) with 2 to 4M $M^{2+}Cl_2 \cdot n\ H_2O$ solutions, respectively. The crystal structures of partly Mg^{2+}- and fully Mn^{2+}-, Cd^{2+}- and Sr^{2+}-exchanged heulandite with the simplified composition $M^{2+}_{4.5}[Al_9Si_{27}O_{72}] \cdot n\ H_2O$ were studied by single-crystal X-ray diffraction at 100 K (Mg) and 293 K (Mn, Cd and Sr). Structure refinements performed in space group *C2/m* yielded R1 values of 4.65%, 4.44%, 4.04% and 4.54%, respectively and the following cation distribution is observed: Mg (ionic radius 0.72 Å) (SHANNON, 1976) occupies the center of the A channel and is coordinated by six H_2O molecules forming two disordered octahedra. The B channel preserves its original Na occupation and only very minor Mg concentrations could be identified within the eight-membered rings. The same type of $M^{2+}(H_2O)_6$ complex in the center of the A channel was found for Mn^{2+} (ionic radius 0.83 Å), and additional Mn^{2+} was found to be dispersed in the A and B channels. Cd (ionic radius 0.95 Å) shows only a very low tendency to form the $Cd^{2+}(H_2O)_6$ complex and is found in the A and B channels. Sr is also about evenly distributed in the A and B channels. Due to the larger ionic radius (ca. 1.3 Å) Sr does not form a $Sr^{2+}(H_2O)_6$ complex in the A channel, but is ninefold coordinated by four framework O and five H_2O molecules. There are two major differences to the previously investigated exchange series of Na, K, Rb, and Cs in heulandite (YANG and ARMBRUSTER, 1996): (1) The small divalent cations are less coordinated by framework O and are preferentially surrounded by H_2O molecules. (2) Small divalent cations are strongly disordered within the channel system and can only partly be located. Divalent cations with large ionic radii (as Sr^{2+}) exhibit a coordination to framework O and H_2O molecules in the A channel.

SHANNON, R.D. (1976): Revised effective ionic radii and systematic studies of interatomic distances in halides and chalcogenides. Acta Cryst., A32, 751–767.

YANG, P., and ARMBRUSTER, T. (1996): Na, K, Rb and Cs exchange in heulandite single-crystals: X-ray structure refinements at 100 K. Journal of Solid State Chemistry, 123, 140–149.

T. Wuest and Th. Armbruster (Bern):

Type locality leonhardite: a single-crystal X-ray study at 100 K. (Poster)

The aim of this study was to investigate the crystal structure of the type locality leonhardite after rehydration and to show possible differences to "normal" laumontite. Laumontite is a monoclinic zeolite with the simplified formula $Ca_4[Al_8Si_{16}O_{48}] \cdot 18\ H_2O$ (space group *C2/m*). BLUM (1843) defined leonhardite as new mineral, distinct to laumontite, because of a different crystal morphology. The type material of leonhardite originates from fissures and cavities in trachytic rocks at Schemnitz, at that time situated in Hungary (nowadays Banska Stiavnica in Slovakia). Subsequently, DELFFS (1843) showed that this

leonhardite has a chemical composition close to laumontite but with less H_2O and more SiO_2. If laumontite is exposed to low humidity, it partially dehydrates at room temperature to a variety with ca. 14 H_2O p.f.u. named leonhardite. This dehydration is reversible by soaking the sample in water (COOMBS, 1952; ARMBRUSTER and KOHLER, 1992).

The investigated sample was taken from a hand specimen collected at Schemnitz that we kindly received from the Museum of Natural History, Vienna (catalogued in 1843). A single-crystal of 0.175 × 0.15 × 0.25 mm in dimension was separated, and submerged in water for several days. Subsequently, the specimen was transferred to an Enraf Nonius CAD4 single-crystal diffractometer (graphite-monochromatized MoKα X-radiation) and quenched to 100 K. Diffraction data were collected at 100 K on two rehydrated crystals.

Natural leonhardite from the type locality has at room temperature space group *C2/m*: a = 14.714(4), b = 13.132(2), c = 7.531(3) Å, β = 111.23°(3), V = 1356.56(75) Å^3. The rehydrated "leonhardite" sample, immediately quenched to 100 K, reveals in addition to the X-ray reflections indexed in space group *C2/m* with a = 14.744(4), b = 13.144(5), c = 7.504(1) Å, β = 110.79(2)° many additional sharp reflections which could not be assigned. When the crystal was stepwise heated, the additional reflections disappeared at ca. 220 K but did not reappear when subsequently cooled down to 100 K. One single crystal X-ray data set was collected at 100 K, based on the *C2/m* cell, in spite of the non-indexed reflections which were ignored. A second data set was measured at 100 K after heating to 240 K thus only the *C2/m* reflections were present: a = 14.743(6), b = 13.132(5), c = 7.503(3) Å, β = 110.81(4)°.

There is no significant difference between the two refined structures. Both show within 3 e.s.d's the same coordinates, displacement parameters, and degree of hydration (15.5 H_2O p.f.u.). The non-indexed reflections, which disappeared at ca. 220 K, may be explained by phase transitions which have been described by GABUDA and KOZLOVA (1995). They found in partially dehydrated laumontite (14.4 H_2O p.f.u.) a phase transition at 230 K related to H_2O order/disorder. After rapid quenching to 100 K, the crystal probably developed additional domains which may represent triclinic twins, while the major portion of the crystal remained in space group *C2/m*. Upon heating above 220 K, the low symmetry domains disappeared and the crystal became homogeneous with *C2/m* symmetry.

For Schemnitz leonhardite, a low occupied K site (occupancy 3%), close to Ca, could be located which agrees with the K site reported by ARMBRUSTER and KOHLER (1992). Electron Microprobe analyses yielded the composition $Ca_{3.59}K_{0.28}Na_{0.08}Mn_{0.01}Fe_{0.01}Al_{7.53}Si_{16.46}O_{48.02} \cdot 13.55\ H_2O$. The refined formula for the rehydrated Schemnitz sample is $Ca_{3.56}K_{0.13}Al_{7.25}Si_{16.75}O_{48} \cdot 15.5\ H_2O$. H_2O positions and also the coordinates of the structural framework atoms are between a laumontite with 17.2 and one with 14.4 H_2O p.f.u. refined by ARMBRUSTER and KOHLER (1992). T–O distances indicate a high degree of Si/Al ordering as found for laumontite (ARMBRUSTER and KOHLER, 1992). The reason why Schemnitz leonhardite could not be completely rehydrated is probably related to the K concentration. Recently STOLZ and ARMBRUSTER (1997) have shown that K in "primary leonhardite" occupies additionally a H_2O site.

ARMBRUSTER, T. and KOHLER, T. (1992): Re- and dehydration of laumontite: A single-crystal X-ray study at 100 K. Neues Jahrbuch für Mineralogie, Monatshefte, 1992, 385–397.

ARTIOLI, G. and STÅHL, K. (1993): Fully hydrated laumontite: A structure study by flat-plate and capillary powder diffraction techniques. Zeolites, 13, 249–255.

BLUM, J.R. and DELFFS, W. (1843): Leonhardit, ein neues Mineral. Poggendorff Annalen der Physik und Chemie, 59, 336–342.

COOMBS, D.S. (1952): Cell size, optical properties and chemical composition of laumontite and leonhardite. American Mineralogist, 37, 812–830.

GABUDA, S.P. and KOZLOVA, S.G. (1995): Guest-guest interaction and phase transitions in the natural zeolite laumontite. Journal of Inclusion Phenomena and Molecular Recognition in Chemistry, 22, 1–13.

STOLZ, J. and ARMBRUSTER, T. (1997): X-ray single-crystal structure refinement of a Na,K-rich laumontite, originally designated "primary leonhardite". Neues Jahrbuch für Mineralogie, Monatshefte, 1997, 131–144.

PETROLOGY: THEORETICAL/EXPERIMENTAL

X. Liu, V. Pokrovskii and Ch.A. Heinrich (Zürich):

Partial molal volumes of NaCl (aq) in high-temperature aqueous fluids with liquid-like to gas-like densities.

Aqueous NaCl solution is more extensively studied experimentally than any other binary fluid system, partly because of the importance of this system for geological processes. In natural magmatic-hydrothermal systems, fluids of extremely variable salinity are common, ranging from hydrous salt melts or brines to vapour-like fluids of lower salinity. In many magmatic-hydrothermal systems associated with ore formation at low to

moderate pressures (< 2 kbar), two NaCl–H_2O rich fluids coexist as immiscible brine + vapour phases. The thermodynamic properties of the salt-bearing vapour phase, in particular, are essential for understanding many geological phenomena, but have been poorly known until now.

Recently, the densities of NaCl solution have been measured to temperatures above 700 K at relatively low pressure (< 400 bar) by MAJER et al. (1991). The extrapolated partial molal volumes of NaCl (aq) from these experimental data, together with the earlier results tabulated by PITZER et al. (1984) and more recent measurements (SIMONSON et al., 1994; MAJER et al., 1988) at temperatures below 600 K, are used to derive a relation for the partial molal volume of NaCl (aq) at infinite dilution that may be extrapolated to very low densities of the solvent H_2O.

There are several formulations to express the partial molal volumes of aqueous species, among which the derivation by chain rule from the definition of partial volume and the one by differentiation from the Gibbs-Duhem relation were extensively used to study the standard partial molal volume at the vicinity of the critical temperature of the solvent (ECKERT et al., 1983; KRICHEVSKII, 1967). We find that using only one of these expressions to fit the experimental data leads to non-trivial relations with respect to density and temperature over the whole range of temperatures and pressures. However, a weighted combination of these two expressions can lead to a simple relation with four adjustable parameters which closely represents the experimental data over a wide range of temperatures (from 298 K to above 700 K) and the pure solvent (water) densities (from 0.1 g/cc to above 1 g/cc). The equation is also tested against the solubility data of quartz because the solubilty measurements of quartz covers a much wider range of temperatures and water densities. With this test it seems likely that the relation can be used confidently up to temperatures of 900 K.

ECKERT, C.A. et al., Fluid Phase Equilibria, 1983, Vol. 14, 167.
KRICHEVSKII, I.R. et al., Russian Journal of Physical Chemistry, Vol. 41, 1332.
MAJER, V. et al., J. Chem. Thermodynamics, 1988, Vol. 20, 949.
MAJER, V. et al., J. Chem. Thermodynamics, 1991, Vol. 23, 213.
PITZER, K.S. et al., J. Phys. Chem. Ref. Data, 1984, Vol. 13, 1.
SIMENSON, J. et al., J. Chem. Thermodynamics, 1994, Vol. 26, 345.

M. Kirschen and Ch. De Capitani (Basel):

Immiscible Silicate Liquids in the CaO–SiO_2–TiO_2–Al_2O_3 System *(see p. 175–178, this issue).*

M. Kunz, G. Fiquet, D. Andrault and D. Häusermann (Zürich, Lyon, Paris, Grenoble):

Mineralogy at extreme conditions.

Almost all minerals, which are stable in the pressure- and temperature-range of the earth's crust have been subject to mineralogical investigations during the past 30 years. This lead to a very detailed understanding of mineralogical and crystal-chemical processes as they are observed on the surface of the earth. A similarly comprehensive database is not yet achieved for phases which are stable in the interior of planets. Due to this lack of experimental data, geophysicists are forced to rely largely on crystal-chemical speculation and computer-aided modelling to explain seismic data in terms of a mineralogical composition of the deep earth. The recent start-up of third generation synchrotron sources such as the European Synchrotron Radiation Facility (ESRF) with its dedicated high pressure beamline is a major step towards an experimental exploration of the mineralogy of the earth's interior.

Experiments are currently performed in situ at high pressures up to 1 Mbar and temperatures of 3000 Kelvin using diamond anvil cells and internal laser-heating at the high pressure beamline (ID30) of the ESRF in Grenoble. This enables direct crystallographic investigation of material at conditions as they occur at the core-mantle boundary. First experiments were done on $MgSiO_3$ perovskite and on Fe.

$(Mg,Fe)SiO_3$ together with (Mg,Fe)O is assumed to be a major constituent of the lower mantle. The aim of our experiment is not only to obtain an accurate equation of state for the region of the core-mantle boundary, but also to test the recently published hypothesis of a decomposition of $MgSiO_3$ perovskite into SiO_2 (stishovite) and MgO (periclase). Our data do not show any evidence for decomposition in the temperature- and pressure range investigated (2500 K, 80 GPa). Comparison between a PREM-model and the equation of state deduced from our data suggest the lower mantle to be composed of 83 vol.% $(Mg_{0.93}Fe_{0.07})SiO_3$ perovskite and 17 vol.% $(Mg_{0.79}Fe_{0.21})O$ magnesiowüstite.

The phase diagram of Fe in the region of the core-mantle boundary is strongly debated. Besides the melting curve of Fe, it is mainly the existence and the possible structure of a b-phase at

pressures above 30 GPa and temperatures between 1500 K and 2500 K which are the subject of recent research. Our data obtained in situ at these conditions suggest indeed the existence of such a phase and we propose an orthorhombic structure with space group Pbcm. The proposed structural model could be confirmed using the Rietveld refinement technique.

Monika Weiss and Peter Ulmer (Zürich):

Stability and phase relations of Ti-clinohumite to 10 GPa.

Ti-Clinohumite is a widespread mineral in Alpine-type ultramafic massifs. It mainly occurs in serpentinized lherzolites and harzburgites, coexisting with olivine, antigorite serpentine, diopsidic cpx, apatite, and chlorite. Ti-clinohumite abundances are generally low, but nevertheless the presence of Ti-clinohumite can have profound geochemical implications. Clinohumites are not only OH-carriers, able to transport and store H_2O deeply into the upper mantle, but they can accommodate considerable amounts of high field strength elements (HFSE), such as Nb, Ta, Zr, Hf in addition to Ti (WEISS, 1997). In order to understand the formation and stability of clinohumite in ultramafic rocks, a series of high pressure experiments were performed on different natural and synthetic clinohumite samples. 4 different compositions were investigated: (1) a natural fluorine-free, titanium-saturated (xTi = 0.46) clinohumite; (2) a natural fluorine-free titanium-bearing (xTi = 0.28) clinohumite; (3) a natural fluorine- and titanium-bearing (xF = 0.47, xTi = 0.19) clinohumite; and (4) a synthetic F-clinohumite.

The experiments were performed in piston cylinder (0.5–3.5 GPa) and multi-anvil apparatus (4–10 GPa). Due to the sluggish reaction kinetics, very long run times were necessary (up to 1200 hours). The different starting compositions were used to investigate the influence of Ti, F and Fe on the stability of Ti-, F-bearing clinohumites. Successful reversal experiments were not possible; the synthesis of crystallographically homogeneous clinohumite was not obtained except for pure F-clinohumite; all other attempts resulted in various humite-like polysomes or other hydrous magnesio-silicates.

The natural F-free, Ti-saturated (1) clinohumite breaks down to olivine + ilmenite + fluid; at pressure greater then 7.8 GPa, Ti-chondrodite forms the low temperature humite mineral instead of Ti-clinohumite. The temperature stability increases from 615 °C at 1 GPa to 1050 °C at 7.8 GPa. The Ti-bearing clinohumite (2) breaks down over an approx. 100 °C wide temperature interval, where Ti-enriched clinohumite (relative to the starting composition) coexists with olivine + rutile + ilmenite + fluid. Fluorine drastically increases the clinohumite stability field: the Ti- and F-bearing clinohumite (3) increases its stability field by more than 300 °C relative to (1) and the Ti-free F-clinohumite (4) by more than 600 °C. Pure F-clinohumite breaks down to fluorine-norbergite plus forsterite.

In summary, increasing titanium stabilises clinohumite to higher pressures and temperatures relative to Ti-undersaturated F-free clinohumites. Fluorine strongly increases the temperature stability of clinohumite.

Fluorine-free Ti-clinohumites are only stable in cold subducted lithosphere, whereas F- and Ti-bearing clinohumites can be stable in subcontinental cratonic mantle. Ti-clinohumite has a higher temperature stability then antigorite serpentine at pressures exceeding 2 GPa. Therefore, Ti-clinohumite is still stable in the ultramafic oceanic lithosphere, when serpentine breaks down and exerts a strong control on the distribution of HFSE in the released fluids. The presence of Ti-clinohumite during the breakdown of serpentine could be responsible for the relative depletion of HFSE in supra-subduction island arc magmas.

WEISS, M. (1997) Clinohumites: A field and experimental study. Diss. ETHZ, Nr. 12202, 201 pp.

J. Konzett and P. Ulmer (Washington, Zürich):

K-richterite: phase relations and stability in the KNCMASH-system and in natural lherzolite. (Poster)

The natural occurrences of K-richteritic amphiboles (Kr) are almost exclusively confined to extremely peralkaline and Al-poor bulk systems, such as lamproites and kimberlitic (MARID-type) mantle xenoliths. Such compositions were approximated by a simplified synthetic *peralkaline* oxide mix with $(K_2O + Na_2O)/Al_2O_3 = 1.71$. Experiments were performed up to 3.0 GPa with an endloaded piston cylinder and from 3.5 to 10 GPa with a Walker-type multi-anvil device. In the peralkaline bulk composition, K-richterite appears between 1.0 and 1.5 GPa coexisting with phl+cpx+fluid and remains stable in the same assemblage to more than 8.5 GPa at 1100 °C. At $P \geq 7$ GPa and $T > 1200$ °C, K-richterite coexists with garnet in an assemblage Kr+gar+cpx+ol+fluid. At 8.0 GPa the upper thermal stability limit of Kr and phlogopite is reached simultaneously between 1300 and 1400 °C with a breakdown assemblage gar+cpx+ol+melt.

In order to study the stability of K-richterite in peridotitic systems, a *subalkaline* composition with $(K_2O + Na_2O)/Al_2O_3 = 0.64$ was prepared. K-richterite stability in this bulk composition is confined to P > 6.5 GPa at 1100 °C and to > 6.0 GPa at 800 °C due to phlogopite breakdown by the reaction phl+cpx+opx = Kr+gar+ol+fluid. In the present experiments, opx is completely removed by this reaction and the stable assemblage at P > 6.5 GPa / 1100 °C is Kr+phl+gar+cpx+ol+fluid. This is not likely in a lherzolite, because opx is much more abundant than phlogopite (usually < 2%). Additional experiments have been performed to test this hypothesis and to delimit the stability of K-richterite and phlogopite in a peridotitic mantle. A synthetic phlogopite-peridotite composition (containing 5% phlogopite) was chosen as the starting composition. The stable assemblage found is phl+gar+opx+cpx+ol+fluid below 6.5 GPa and Kr+gar+ cpx+opx+ol+fluid at P ≥ 6.5 GPa.

This experimental study reveals that K-richterite amphibole is a stable mineral from 1.0 to > 9 GPa in low temperature peralkaline compositions, such as MARIDs in the upper mantle. In contrast, K-richterite only occurs at pressures ≥ 6.5 GPa in peridotite compositions, where it replaces phlogopite as the K- and H_2O-carrier. The restricted temperature stability of < 1400 °C at 8.0 GPa limits the occurrence of K-bearing phases in the lower part of the upper mantle (> 6.5 GPa) to cold regions with temperatures less than the average current mantle adiabat (ACMA) such as cratonic subcontinental lithosphere.

PETROLOGY: MAGMATIC, VOLCANIC

G. Armando, J. Hernandez and B. Villemant (Lausanne, Paris):

Jurassic magmatism in the Central High Atlas (Morocco): emplacement and evolution of the gabbroic layered intrusion of Jebel Hayim Massif. (Poster)

The Jebel Hayim Massif belongs to a suite of alkaline to transitional intrusive massifs scattered in the axial zone of the Moroccan Central High Atlas and formed during a Middle to Upper Jurassic transtensional phase. The country-rock is locally strongly deformed and the style of deformation evidences a sinistral strike-slip regime which was contemporaneous to magma emplacement (Oxfordian). Magma rose up into the upper crust where it solidified within Triassic to Early Jurassic sedimentary sequences at the bottom of the High Atlas cover. At present it is emplaced within Bajocian to Bathonian sediments and is the result of a post-magmatic tectonic extrusion. The Jebel Hayim Massif is made of two gabbroic layered complexes (JH1 and JH2) overlain by pneumatolytic gabbros and cross-cut by monzonitic to syenitic dikes. Both complexes are comprised by a lower series made up of troctolites and by an upper series made up of oxide-rich gabbros and ol-gabbros, respectively. The contacts between lower and upper series are horizontal and primary. Troctolites and ol-gabbros are cumulates with olivine, plagioclase and augite as early cumulus phases, and ilmenite, biotite and kaersutite as late interstitial phases. Both display modal and cryptic layering with olivine content decreasing from bottom to top as well as the MgO content of all mineral phases. The oxyde-rich gabbros are characterized by abundant magnetite (10%), scarcity of olivine, low MgO and flow texture, and they do not display neither modal nor cryptic layering. The composition of liquids was calculated for representative rock types using the trace element content in olivine, plagioclase and clinopyroxene, and selected sets of partition coefficients. Calculated liquids indicate that the gabbro evolution was not continuous and not linear, and that different parental magmas were at the origin of different series. In particular, different degrees of partial melting are invoked to explain the variations of incompatible elements (Hf, Ta, REE and Th) abundance and a early differentiation stage at depth is necessary to explain the relative low content of MgO (< 9%) and the variations of compatible elements (Ni and Cr) abundance. In particular, oxide-rich gabbros are depleted in both compatible elements and incompatible elements and this discrepancy is attributed to a larger degree of partial melting (2.5%) relative to troctolites and ol-gabbros and to a large precipitation of olivine and chromite at depth (13% of fractional crystallization). Troctolites and ol-gabbros parental magmas could result from a degree of partial melting ranging from 0.6% for JH2 troctolites to 1.2% for JH2 ol-gabbros to 1.8% for JH1 troctolites.

F. Bussy, D. Délitroz, R. Fellay, J. Hernandez (Lausanne):

The Pormenaz monzonite (Aiguilles-Rouges, Western Alps): an additional evidence for a 330 Ma-old magnesio-potassic magmatic suite in the Variscan Alps. (Poster)

The Pormenaz monzonite is located about 7 km NW of Chamonix (F), in the Aiguilles-Rouges Massif, which represents, together with

the other External Crystalline Massifs, the best preserved witnesses of the pre-Mesozoic history of the western Alps. The Pormenaz monzonite is a 1.4 by 2.5 km porphyritic mass, funnel-shaped in vertical cross section, with large pink K-feldspar megacrysts in a dark green amphibole+biotite-rich matrix. It intruded within a complex series of lower Paleozoic(?) gneisses, as well as metagrauwackes of supposedly Lower Carboniferous age according to their weak metamorphic grade. The lowest levels of exposure show strongly deformed rocks; they suggest a syntectonic emplacement of the magma followed by post-crystallization mylonitic deformations along a long-lasting subvertical N–S strike-slip fault (DOBMEIER, 1995).

The main porphyritic facies has a monzonitic to monzodioritic composition and typically consists of orthoclase (5–40%), oligoclase (An27, 25–55%), quartz (0–17%), Mg-hornblende (< 13%), Mg-biotite (10–28%), abundant titanite (up to 2.5%), apatite, zircon and magnetite. Plurimetric bodies of durbachite are found as quartz-free autholithic enclaves high in hornblende (30–55%), biotite (15–25%), Ba-rich K-feldspar (20–25%) and titanite (up to 5%). Leucocratic facies and aplitic dykes occur in the periphery. Whole-rock chemistry shows strong affinities with calc-alkaline magnesio-potassic (Mg–K) series, such as those described e.g. in Corsica, the Vosges or the Bohemian Massif (e.g. COCHERIE and ROSSI, 1995). Characteristic features are high to very high concentrations in LIL-elements like K_2O (3.4–7.2%), Rb (200–300 ppm), Ba (1200–3300 ppm), Sr (500–900 ppm); in MgO (2.5–4.6%) and transition elements like Cr (100–200 ppm), Ni (20–90 ppm) and V (100–150 ppm), and in incompatible elements like LREE (100–230 ppm Ce), Zr (280–430 ppm) and Th (20–50 ppm). These features and the presence of durbachitic enclaves of lamprophyric affinity suggest a metasomatized mantellic source.

Zircons display simple morphologies with well developed {100} and {101} faces (high T and A indexes of 633 and 607, respectively), fine and oscillatory chemical zoning, rather low U, Th and Hf concentrations typical of zircons from calc-alkaline suites, and scarce inherited cores. U–Pb isotope dilution analyses on 3 small multigrain fractions yielded a concordant age of 333 ± 2 Ma. This age is strikingly similar to that of all other dated Mg–K granitoids in the External Crystalline Massifs, including the Pelvoux (331 Ma), Belledonne (332 Ma) and the Aar (334 Ma), whereas Mg–K rocks in adjacent areas are sightly older at 340 Ma (Vosges) and 337 Ma (Corsica) (see review e.g. in DEBON et al., 1998). All these intrusions seem to define an «isochron Mg–K magmatic line along the Variscan belt» (ROSSI and COCHERIE, 1995). This feature probably reflects a major geotectonic structural control, related to: (1) the location and geometry of a Lower Paleozoic subduction slab, which metasomatized the overlying mantle wedge in a band parallel to the Gondwana-Laurasia continental suture; (2) crustal-scale transcurrent faults linked to Visean syn-convergent extensional zones. The latter favored partial fusion of the underlying high-K lithospheric mantle and generated the same kind of magmas simultaneously all along the Alpine segment of the Variscan chain, with local variations related to the nature of the interacting continental crust.

COCHERIE, A. and ROSSI, P. (1995): Respective roles of source composition and melting conditions in the high-K content of some magmas: geochemical constraints. In "The origin of granites and related rocks" 3rd Hutton symposium, Abstracts. U. S. geol. Survey circ. 1129, 36–37.

DEBON, F., GUERROT, C., MÉNOT, R.P., VIVIER, G. and COCHERIE, A. (1998): Late Variscan granites of the Belledonne massif (French western Alps): a lower Visean magnesian plutonism. Schweiz. Mineral. Petrogr. Mitt. 78, 67–85.

DOBMEIER, C. (1996): Die variskische Entwicklung des südwestlichen Aiguilles-Rouges-Massivs (Westalpen, Frankreich). Ph. D. Thesis, Mém. Géol. Lausanne, 29, 191 pp.

ROSSI, P. and COCHERIE, A. (1995): A belt of high-K plutonic rocks related to crustal extension: evidence from the European Variscan. In: "The origin of granites and related rocks" 3rd Hutton symposium, Abstracts. U.S. geol. Survey circ. 1129, 128–129.

M.A. Dungan (Genève):

Research activities in volcanic petrology and volcanology at the University of Geneva.

Our primary research goals are to advance the understanding of magma differentiation processes, particularly in open systems, and to determine their rates. The objects of our studies are primarily calc-alkaline systems ranging from Tertiary calderas and ignimbrites of the westem USA (San Juan volcanic field, Colorado; Rattlesnake Tuff, Oregon), to late Pleistocene and recent volcanism of Central (Volcán Arenal, Costa Rica) and South America (Volcán Tatara-San Pedro, Chile). We emphasize the importance of developing a precise eruptive chronostratigraphy by combining field, photogrammetric, geochronologic, and paleomagnetic studies (SINGER et al., 1997; LIPMAN et al., 1996). We undertake comprehensive petrologic investigations of large volcanic systems which stress integration of multiple kinds of chemical and isotopic data.

In order to develop the capacity for making a unique contribution to such problems, we have established a Nomarski DIC microscopy laboratory with image processing capabilities, and are using it primarily for studies of igneous plagioclase. This work has led us in the direction of determining new plag/melt partition coefficients using existing experimental charges, which we are using to invert trace element compositions of natural plagioclase, determined by SIMS, to coexisting liquid compositions. The integration of chemical data with textural insights from NDIC microscopy enables us to estimate continuous and discontinuous liquid evolution paths in subvolcanic magma chambers (SINGER et al., 1995; FEELEY and DUNGAN, 1996).

Our second new analytical tool is a $^{40}Ar/^{39}Ar$ dating laboratory dedicated to achieving high-precision ages of very young volcanic rocks using a variety of materials (whole-rocks, rhyolitic glass, and minerals). We hope to determine extremely precisely dated eruptive histories for Tertiary and late Pleistocene volcanic systems which will enable us to address problems such as magma production rates. Brad Singer has expanded the role of this laboratory into calibration of the geomagnetic and astronomical time scales (SINGER and PRINGLE, 1996), dating of ore deposits in support of Fontboté's group, and into the area of Pleistocene paleoclimatology (see abstract). To further augment the function of this laboratory, we have recently acquired both UV and IR laser probes that will permit both spot and bulk step-heating analyses.

The second half of this presentation will feature a discussion of new results from the Fish Canyon Tuff, Colorado, one of the largest known ignimbrites (see abstract). The Fish Canyon Tuff has been a subject of controversy for more than a decade as the result of geothermometric-geobarometric studies by Whitney and Stormer, wherein they suggest that the Fish Canyon phoenocryst assemblage equilibrated at lower crustal pressures (7–9 kbar). The thermodynamic model used to estimate these pressures and the dynamic implications of a caldera eruption linked to a magma chamber at this depth have been sharply criticised. Our new observations suggest a multistage, upper crustal origin for the Fish Canyon magma, and provide explanations for the apparently erroneous results of Whitney and Stormer.

FEELEY, T.C. and DUNGAN, M.A. (1996): Compositional and dynamic controls on mafic-silicic magma intercractions at continental arc volcanoes Evidence from Cordon El Guadal, Tatara-San Pedro complex, Chile. J. Petrol., 37, 1547–1577.

LIPMAN, P.W., DUNGAN, M.A., BROWN, L. and DEINO, A. (1996): Recurrent eruption and subsidence at the Platoro caldera complex, southeastern San Juan volcanic feld, Colorado: New tales from old tuff. Geol. Soc. Amer. Bull., 108, 1039–1055.

SINGER, B.S. and PRINGLE, M.S. (1996): Age and duration of the Matuyama-Bruhnes geomagnetic polarity reversal from $^{40}Ar/^{39}Ar$ incremental-heating analyses of lavas. Earth Plan. Sci. Lett., 139, 47–61.

SINGER, B.S., DUNGAN, M.A. and LAYNE, G.D. (1995): Textures and Sr, Ba Mg, Fe, K, and Ti compositional profiles in volcanic plagioclase: Clues to dynamics of calc-alkaline magmas. Amer. Min., 80, 776–798.

SINGER, B.S., THOMPSON, R.A., DUNGAN, M.A. and FEELEY, T.C. and others (1996): Volcanism and erosion during the past 930 ka at the Tatara-San Pedro complex, Chilean Andes. Geol. Soc. Amer. Bull., 109, 127–142.

Fidel Costa, Brad Singer, Michael Dungan (Genève):

Boundary layer processes of magma reservoirs: insights from SIMS studies of plagioclase. (Poster)

Our knowledge about physico-chemical processes responsible for differentiation that occurs in magma reservoirs remains limited. Nonetheless, there is increasing evidence that boundary layers of magma chambers may play a very important role in differentiation (e.g., JAUPART and TAIT, 1995). Magmatic differentiation processes may be preserved in crystal cumulates or crystal-melt mushes, that may record crystal growth and melt segregation within cooling, solidifying boundary layers of magma chambers. BROPHY et al. (1996) used major and trace element zoning of plagioclase in mafic glass-bearing cumulate inclusions to propose an origin for the compositional gap (Daly gap) common among calc-alkaline volcanoes. In this same sense, we have undertaken a major and trace element study of plagioclase from a suite of glass-bearing mafic crustal xenoliths, interpreted as crystal mushes, incorporated from the margin of the magma chamber which produced the dacitic lava flow hosting these inclusions at Volcán San Pedro, a Holocene vent in the Tatara-San Pedro volcanic complex, Chilean Andes (SINGER et al., 1997).

Electron and ion microprobe data were obtained from plagioclase in three glass-bearing gabbroic xenoliths. Main petrographic features are: (1) 25–35% zoned plagioclase that grew both pre- and post-amphibole, (2) 1 to 10% interstitial residual glass, (3) 12 to 33% of primary amphibole. Empirical relations derived by BLUNDY and WOOD (1991) and BINDEMAN et al. (1997) were used to calculate melt compositions in equilibrium with plagioclase. Most plagioclase crystals have cores of An_{85-78} and rims of An_{45-26}, separated by an abrupt compositional change ranging from 30 to 40 anorthite mol%. From the inner to

the outer part of the core, measured Ti, K, Sr, Ba, Y, La and Ce increase regularly, Mg decreases, while Fe* stays constant. Rims do not show any systematic enrichment or depletion trend. Rims are richer in K, Sr, Ba, La, Ce, have higher La/Ce and La/Y ratios, and are poorer in Mg, Ti, Fe* and Y, than cores. The fact that these large compositional changes occur in the scale of a hundred microns suggests that an abrupt physical change occurred in the magmatic system. Three possibilities are envisaged: (1) a large pulse of crystallization over a small temperature interval, (2) replenishment of the interstitial melt by more evolved liquid, and (3) a combination of (1) and (2).

Melts that precipitated the plagioclase cores, decrease from 6 to 2 wt% MgO. This, coupled with increasing K, Sr, Ba, Y, La, and Ce, and constant La/Ce and La/Y ratios, is interpreted to reflect the early crystallization of olivine and orthopyroxene. In addition, we note: (1) large enrichment factors between cores and rims of La (4.8–5.8-fold), Ce (2.9–3.4), K (2–3), La/Ce (1.5–2), (2) depletion of Ti (0.05–0.1) and Y (0.06–0.2) in the rims, and (3) a change in La/Ce ratios from 0.3 in cores to 0.7 in the rims. These features lead us to suggest that a highly differentiated melt replaced the original interstitial melt of the crystal-liquid mush. Furthermore, the La/Ce and La/Y ratios and the low Ti contents of this melt suggest extensive crystallization of amphibole plus Fe–Ti oxides, consistent with the mineralogy of the inclusions. The proposed two-stage growth of plagioclase, apparently separated by influx of new liquid into the mostly crystalline mush, and the major role of amphibole in derivation of evolved liquids, set the Volcán San Pedro inclusions apart from the Medicine Lake inclusions studied by BROPHY et al. (1996). Medicine Lake cumulate plagioclases recorded uninterrupted monotonic crystallization histories that require all evolved rhyolitic liquid to escape the crystal-liquid mush; our data suggest that this may not always be the case.

BINDEMAN, I.N., DAVIS, A.W. and DRAKE, M.J. (1997): Ion microprobe study of plagioclase-basalt partition experiments at natural concentration levels of trace elements. Geochim. Cosmochim. Acta (in review-personal communication).

BLUNDY, J.D. and WOOD, B.J. (1991): Crystal-chemical control on the partitioning of Sr and Ba between plagioclase feldspar, silicate melts, and hydrothermal solutions. Geochim. Cosmochim. Acta, 55, 193–209.

BROPHY, J.G., DORAIS, M.J., DONNELLY-NOLAN, J. and SINGER, B.S. (1996): Plagioclase zonation styles in hornblende gabbro inclusions from Little Glass Mountain, Medicine Lake volcano, California: implications for fractionation mechanisms and the formation of composition gaps. Contrib. Mineral. Petrol., 126, 121–136.

JAUPART, C. and TAIT, S. (1995): Dynamics of differentiation in magma reservoirs. J. Geophys. Res., 100, 17615–17636.

SINGER, B.S., THOMPSON, R.A., DUNGAN, M.A., FEELEY, T.C., NELSON, S.T., PICKENS, J.C., BROWN, L.L., WULFF, A.W., DAVIDSON, J.P. and METZGER, J. (1997): Volcanism and erosion during the past 930 k.y. at the Tatara-San Pedro complex, Chilean Andes. Bull. Geol. Soc. Am., 109, 127–142.

M. Dungan, P. Lipman and O. Bachmann
(Genève, Menlo Park):

Origin of the Fish Canyon magma body: central San Juan volcanic field, Colorado, USA. (Poster)

Restudy of the Fish Canyon Tuff demonstrates that: (1) eruptive volume from the La Garita caldera (85 × 30 km) was ~5,000 km^3, (2) caldera collapse was preceded by eruption of 200–300 km^3 of spatter-fed lava that provides reliable magma compositions, (3) erupted homogeneous dacite (68–69% SiO_2) was in contact with a large subjacent intrusion of andesitic magma, and (4) feldspar-liquid disequilibrium is comparable to that which characterizes strikingly resorbed quartz. The latter observation explains formerly controversial thermo-barometric discrepancies, may pose problems for the utilization of Fish Canyon minerals as geochronologic standards, and places important constraints on the origin of the Fish Canyon magma body.

The Fish Canyon magma body formed by a mechansim which is distinct from the origin of most granitoids (deep partial melting-segregation-ascent) or common silicic volcanics (shallow differentiation from more mafic magma). Large poikilitic sanidines enclose plagioclase, quartz, and other minerals; grain-boundary melting along contacts with mineralogically diverse inclusions is often at an advanced stage. Thus, quartz resorption reflects a major thermal event, not a response to decreasing pressure during magma ascent (contraction of SiO_2 stability relative to feldspars). Partial diffusive equilibration adjacent to melt pockets, and along sanidine grain margins, has produced large compositional gradients that truncate pre-existing zoning in sanidine. Rare, intact plagioclase-sanidine contacts apparently preserve up-temperature diffusion gradients superimposed on down-temperature gradients. Unmelted granophyric granitoid fragments in late-erupted intracaldera tuff are characterized by mineralogy and mineral chemistry identical to those of "phenocrysts" in tuff and precaldera magmas. These granitoid blocks apparently were scavenged from magma chamber margins during the waning stages of the eruption. Such features indicate that

the Fish Canyon magma reservoir formed either by rapid, shallow partial fusion of an existing batholith, or by partial remelting of the solidified margins of a long-lived magma chamber.

S. Pilet, A. Collomb, J. Hernandez et P. Nehlig (Lausanne, Orléans):

Evolution magmatique du volcanisme tertiaire du Cantal (Massif central français): nouvelles données minéralogiques et chimiques.

Magmatic evolution of Tertiary volcanism of Cantal (Massif Central, France): new mineralogic and chimical data. (Poster)

Le massif du Cantal est un stratovolcan de 60 km de diamètre dont l'activité s'étend du Miocène au Pliocène. Ses laves se divisent en deux séries alcalines allant des basaltes à des termes évolués sur- et sous-saturés. Nous ne décrirons ici

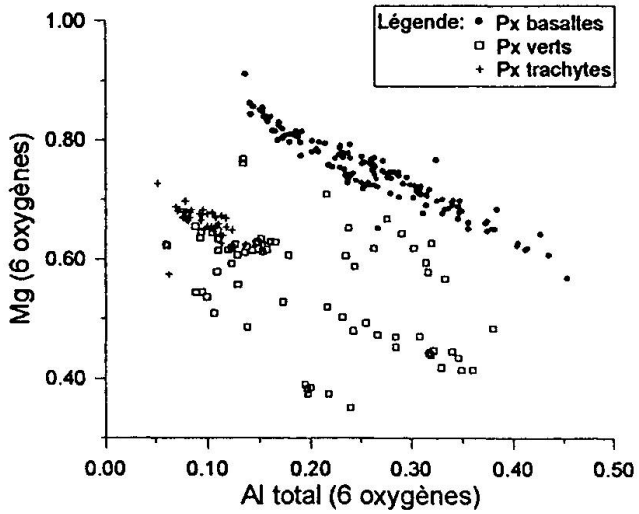

Fig. 1 Diagramme Al total – Mg.

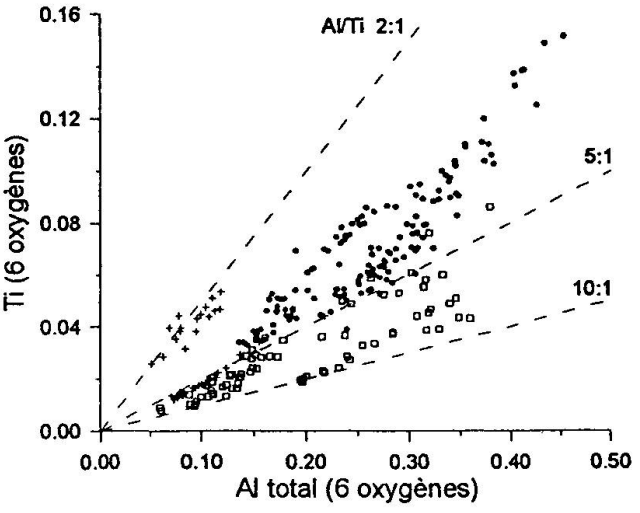

Fig. 2 Diagramme Al total – Ti.

que l'évolution d'un type de pyroxène, illustrant l'évolution polybarique-polythermique des laves les plus évoluées. Dans les basaltes du Cantal, on rencontre fréquemment au cœur des phénocristaux d'augite des cœurs verts dont les teneurs en Hd varient de 35 à 70% alors que les bordures n'en contiennent que 25%. Les pyroxènes verts des trachytes et trachyphonolites ont pour leur part des teneurs en Hd de 50%.

La comparaison de la composition des pyroxènes verts dans l'ensemble de la série montre une évolution du rapport Al/Ti allant de 5 dans les trachytes à plus de 10 dans les basaltes (Fig. 2). De même, on observe une variation continue des teneurs en Na, Mg (Fig. 1), etc. THY (1991) a montré que le rapport Al/Ti des pyroxènes dépendait de la pression. Les variations de composition observées dans les cœurs verts des pyroxènes des laves du Cantal nous permettent de proposer une cristallisation à des pressions comprises entre 5 et 11 Kb (Fig. 2), dans des liquides de composition trachytique ou trachyphonolitique. Les pyroxènes verts des coulées ou des dômes trachytiques ont une composition en accord avec une cristallisation à BP et dans la continuité d'évolution des précédents (Fig. 2). Ces données nous permettent de proposer, pour les laves du Cantal, une différenciation des liquides magmatiques (et en particulier de certains termes évolués) à plusieurs niveaux dans la croûte, situés entre 2 et 30 km. Ce modèle est proche de celui proposé par DUDA et SCHMINCKE (1985), à partir de pyroxènes analogues, pour les laves de l'Eifel.

A. Hobson, F. Bussy and J. Hernandez (Lausanne):

Shallow level gabbro anatexis during contact metamorphism (Fuerteventura Basal Complex, Canary Islands). (Poster)

The Fuerteventura Basal Complex (BC) is a distinct unit formed of igneous rocks and of a series of Jurassic to Tertiary clastic sediments which form the substratum of the island. The BC's plutonic rocks consist of five Miocene (~ 20 Ma) alkaline nested intrusions and dykes, emplaced within a very short time span. One of these intrusions, the gabbro-pyroxenite PX1 pluton, thermally metamorphosed and deformed its country rock the Tierra Mala (TM) intrusion, which consists of gabbros and pyroxenites locally fenitized by carbonatite and ijolite dykes. The basic intrusions are all elongated in a NNE–SSW direction and reflect an E–W extension of the lithosphere.

Gabbroic migmatites, cropping out in 300 m-wide zone along the contact between PX1 and

TM, result from the deformation and partial melting of the TM rocks during emplacement of PX1. The migmatites are characterized by a dense network of anatectic leucocratic veins, rimmed by narrow dark selvages, in a dark fine-grained recrystallized matrix. The veins are enriched in P, Sr, LREE,... relative to the unaffected T.M. rocks. They contain elongate undeformed An_{30-50} plagioclase and minor Ti-augite forming a comb-like structure. The inter-vein dark restite is a polygonal assemblage of magnetite ± cpx ± hbl ± bi ± ti ± ilm. We separate the veins into two groups according to their orientation. It appears that both groups of veins can be directly related to the transpressive stress field induced by the emplacement of PX1 and are not the result of a regional deformation. The general context being one of lithospheric extension at the time of formation of the BC, we now know that this extensive regime stopped at least during emplacement of PX1.

Anatexis in the contact aureole cannot be accounted for only by heat transfer from the intruding pluton as both PX1 and its country rock are gabbroic. The presence of a fluid phase as well as a deformation event respectively helped lower the solidus T° and triggered the segregation of the resulting melt. The trace element composition of the recrystallized rocks proves the existence of a fluid phase. Mobilization of syenitic rocks at depth along the contact could have provided these fluids. Transpressive shearing along the contact is evidenced by the presence and orientation of the leucocratic veins in the migmatites. This deformation event probably favored penetration of the syenitic fluids in the contact aureole and induced segregation of the plagioclase melt. From the absence of any solid state deformation in the vein crystals, we can infer that deformation ceased before crystallization of vein material was complete.

This exceptional example of a shallow-level anatexis of gabbros results from the unusual conjunction of a) a high heat flow related to multiple mafic intrusions, b) the lowering of solidus T° enhanced by alkaline fluids and c) local transpressive shearing due to magma emplacement, during a break of the regional lithospheric extension.

M.J. Streck (Genève):

Evolution of large silicic magma chambers: insights from the Rattlesnake Tuff, Oregon. (Poster)

The existence of large (100–x000 km^3), single dacite to rhyolite magma chambers is most dramatically documented through voluminous ignimbrites since they represent snapshots in the life of physically contiguous magma. Voluminous ignimbrites are therefore ideal for studying magmatic processes of large silicic magma batches that pose many unanswered questions regarding their generation, differentiation, and storage.

In general, silicic magma stored only a few kilometers deep below the surface is thought to be hindered from solidifying before erupting through heat released from basaltic magma, in turn accumulated somewhere beneath the silicic chamber. Basaltic magma is also thought to play materially a major role from early on in the evolution of dacite to rhyolite magma as parental magma for fractional crystallization, as hybridization agent during crustal melting, or as mixing member. Thus, large quantities of basaltic magma appear intimately linked to silicic volcanism for which the evidence is generally very sparse. On the other hand, strong trace element zonation within many voluminous rhyolitic ignimbrites imply large crystal piles are simultaneously left at depth during differentiation.

The 7 Ma Rattlesnake Tuff from eastern Oregon represents a magma system from which voluminous (~ 280 km^3) crystal-poor high-silica rhyolites and parts of the intermediate to basaltic underpinning to the rhyoltic portion of the magma chamber erupted. High-silica rhyolite pumices cluster in 4 to 5 compositional groups which are discerned best by trace elements such as La, Eu, Ba, Zr(Hf), Ta(Nb). Major element variations are minor but consistent with Si increasing and Fe, Ti, Mg, and Ca decreasing with degree of differentiation. Modal mineralogy, mineral chemistry, and partition coefficients also change progressively with increasing degree of differentiation. The diversity of high-silica rhyolite compositions is likely the product of successive fractionation processes occurring along the margins of the magma chamber whereas the least evolved high-silica rhyolite magma is possibly the product of dehydration melting.

Dacite pumices and a variety of mafic inclusions reveal the nature of the mafic root zone. Quenching and mingling textures with the host pumices indicate that basaltic inclusions are cognate. Dacite magma formed at the interface between high-silica rhyolites and underlying basaltic andesite magma and was generated by mixing of these two components. Basaltic andesite magma is fractionated and enriched in trace elements compared to regional primitive high-alumina olivine tholeiite (HAOT) lavas. Basaltic andesite magma is interpreted to have evolved from HAOT's through fractionation, recharge, and possibly assimilation while being stalled underneath a silicic cap. Evidence for the input of primitive HAOT is found in inclusions containing fresh Fo_{80} olivines.

Crystal-rich, granular or cumulitic, inclusions indicate that more solidified parts of the mafic root zone were also erupted.

METAMORPHIC PETROLOGY

M. Engi, M. Thüring and T. M. Tóth (Bern):

Tertiary Metamorphism in the Central Alps: Why and When?

While the Central Alps are a textbook example of regional metamorphic zoning, it is far from understood, how this fairly simple zonal pattern evolved. Tectonic and geophysical studies (e.g. PFIFFNER et al., 1997) provide a kinematic framework for the quantitative simulation of the thermal evolution. We report on results from lithospheric scale (2-D) finite element modelling. Adaptive grid techniques were used to accommodate tectonic mass flow, and a full range of thermal effects is included in the description. The central goals of this study were (a) to gain insight into the thermal consequences of the tectonic evolution, and (b) to compare the predicted P-T-t paths with results from petrological and geochronological studies in the Central Alps.

Our simulations explicitly incorporate movements that resulted in the present orogenic structure of the Central Alps; kinematic parameters were based on SCHMID et al. (1996). Three main phases are recognized: (A) subduction (Upper Cretaceous to Middle Tertiary), (B) collision/ rapid exhumation stage (35–23 Ma), (C) slower exhumation (ongoing). During phase (A), the geometry of isotherms strongly reflects the effects of advection, the 500 °C isotherm (I_{500}) being subducted to a depth of 60 km. Upper crustal units present as nappes in the Central Alps underwent prograde metamorphism during this phase, with high (but quite variable) $\Delta P/\Delta T$ ratios. The sudden slowdown of plate-tectonic convergence around 40 Ma ago lead to a conductive relaxation of the earlier isotherm constellation, with I_{500} rising at a rate of 5 km/Ma. This effect appears to be the chief cause of the pronounced thermal overprint in the Central Alps. For example, T_{max} was reached in the northern Lepontine at about 36 ± 2 Ma as a consequence of slab-breakoff (~ 40 Ma), reduction of the subduction window, reduced advective cooling, and locally a reversed ("melon-pit") advection.

Thermobarometric results from ENGI et al. (1995) and TODD and ENGI (1997) and our evaluation of thermochronological data from the literature, and in part substantiated by our own chemical (Th–U–Pb) dates on monazites, paint a reasonable and coherent picture of the sudden change in the PTt evolution that shaped the amphibolite facies dome in the Central Swiss Alps. Thermal models for this type of transition from subduction to collision tectonics must take into account the temporally variable effects of advective and denudation processes. In the typically complex geometric situations encountered in such belts, adaptive grid finite element techniques appear to be an adequate tool for these purposes.

ENGI, M., TODD C.S. and SCHMATZ, D.R. (1995): Tertiary metamorphic conditions in the eastern Lepontine Alps. Schweiz. Mineral. Petrogr. Mitt. 75, 347–369.

PFIFFNER, O.A., LEHNER, R., HEITZMANN, P., MÜLLER, ST. and STECK, A. (eds) (1997): Deep Structure of the Swiss Alps. Results of NRP 20. Birkhäuser, Basel. 380 pp.

SCHMID, S.M., PFIFFNER, O.A., FROITZHEIM, N. and SCHÖNBORN, G. and KISSLING, E. (1996): Integrated cross sections and tectonic evolution of the Alps along the eastern traverse. Tectonics 15/5, 1036–1064.

TODD, C.S. and ENGI, M. (1997): Metamorphic field gradients and tectonic processes in the Central Alps. J. metam. Geol. 15, 513–530.

D. Gebauer and D. Rubatto (Zürich):

35 Ma old UHP-metamorphism of the Dora Maira Massif and other Tertiary HP- and UHP events in the Central and Western Alps: geodynamic consequences.

Ion-microprobe data are reported for zircons extracted from a whiteschist (pyrope quartzite), a jadeite-rich layer as well as a phengite schist within a whiteschist, a 15 cm big pyrope megablast within a coarse grained pyrope quartzite as well as a biotite-phengite gneiss, the metagranitic country-rock of the whiteschists. All mentioned rock types can be shown to have undergone HP- or UHP-metamorphism with maximum P-T conditions reaching 37 kbar at about 800 °C (SCHERTL et al., 1991). Except for this biotite-phengite gneiss, zircons from all other analyzed rocks contain metamorphic or even magmatic-like domains recrystallized, respectively newly formed at 35 Ma.

Narrow, 35 Ma old metamorphic domains also occur along or around apparent inclusions of coesite and high-Si phengite. The host zircons are oscillatory zoned and formed magmatically at ca. 275 Ma. Thus, these "UHP-inclusions" must have entered the zircons along cracks close to the UHP-peak causing partial or complete recrystallization of the magmatic zircon domains. They were then armoured by the surrounding zircon and thus they could survive retrogression during exhumation. Ca. 275 Ma is the most probable age of the magmatic protoliths of all analyzed rock types. The data suggest that the protolith of the

whiteschists are the Permian granitoid country-rocks that were locally metasomatized during rift-related fluid circulation and shearing to form leucophyllites around 210–260 Ma ago (GEBAUER et al., 1997).

The data do not supply any evidence for a geological event around 100 Ma, the "age" of UHP-metamorphism as inferred from conventional, multigrain zircon dating (PAQUETTE et al., 1989) or various Ar-dating techniques (e.g. MONIÉ, 1984; SCAILLET et al., 1990, 1992 or MONIÉ and CHOPIN, 1991). The existence of oscillatory zoned 35 Ma old zircons as well as resorbed zircons confirms the conjecture of SCHERTL et al. (1991) that partial melting occurred during subduction zone metamorphism. It further argues strongly against the assumption that greenschist facies conditions were not exceeded in the Tertiary. Instead, the ion-probe data support the U–Pb and Sm–Nd data of TILTON et al. (1991) that suggested a Tertiary (38 Ma) UHP-metamorphism.

Including existing mica and fission track ages of the dated rocks (e.g. GEBAUER et al., 1997), exhumation and cooling rates can be calculated. The resulting values of ca 20–24 km/Ma (or 20–24 mm/y) at an average cooling rate of ca 85–100 °C/Ma are similar to those for the Adula nappe in the Central Alps (GEBAUER, 1996) or for HP-rocks of the Himalaya (SPENCER and GEBAUER, 1996). The exhumation related, geothermal gradient yields ca 4 °C/km for the dated UHP-rocks. This is in excellent agreement with data based on retrograde mineral reactions (SCHERTL et al., 1991). Thus, heating and cooling rates during subduction and exhumation were of similar magnitude causing a very narrow P-T-t loop at plate tectonic speeds.

The 35 Ma age of UHP-metamorphism of the Dora Maira Massif is in very good agreement with SHRIMP-ages for HP-or UHP metamorphism of the Central Alps (Alpe Arami and Cima di Gagnone, Adula-Cima Lunga nappe; GEBAUER, 1994 and 1996). As further SHRIMP-ages for HP- and UHP metamorphism of the Sesia Zone (ca. 65 Ma) and the Zermatt-Saas Fee ophiolites (ca. 44 Ma) are clearly older (e.g. RUBATTO and GEBAUER, 1997), the concept of one very long lasting subduction episode, starting as early as in the Early Cretaceous, has to be abandoned. Instead, the new data favour successive closure of basins from the SE to the NW. In such a scenario, the Sesia Zone, probably a rift-related, thinned continental fragment or even a microcontinent derived from the northern part of the Apulian margin, was subducted first around the Cretaceous/Tertiary boundary. The oceanic crust of the Zermatt-Saas Fee ophiolites to the NW was the next unit to be subducted in the Middle Eocene (ca. 44 Ma). With the final subduction of the European margin at ca. 35 Ma, convergence slowed down considerably and was followed immediately by very rapid exhumation. Thus, similar to the European Variscides (GEBAUER and GRÜNENFELDER, 1982), also the Alps formed as a result of successive closure of basins with variable degrees of oceanization.

GEBAUER, D. (1994): A P-T-t path for some high-pressure ultramafic/mafic rock associations and their felsic country-rocks based on SHRIMP-dating of magmatic and metamorphic zircon domains. Example: Central Swiss Alps. Extended abstract version for 16th general meeting of IMA, Pisa, Italy, Sept. 4–9, 139–140.

GEBAUER, D. (1996): A P-T-t Path for an (Ultra?-) High-Pressure Ultramafic/Mafic Rock-Association and its Felsic Country-Rocks Based on SHRIMP-Dating of Magmatic and Metamorphic Zircon Domains. Example: Alpe Arami (Central Swiss Alps). In: BASU, A. and HART, S. (eds): Earth Processes: Reading the Isotopic Code, Geophys. Monogr. Vol. 95, 307–329, AGU, Washington, D. C.

GEBAUER, D. and GRÜNENFELDER, M. (1982): Geological development of the Hercynian Belt of Europe based on age and origin of high-grade and high-pressure mafic and ultramafic rocks. Extended Abstract. Fifth International Conference on Geochronology and Isotope Geology. Japan.

GEBAUER, D., SCHERTL, H.-P., BRIX, M. and SCHREYER, W. (1997): 35 Ma old ultrahigh-pressure metamorphism and evidence for very rapid exhumation in the Dora Maira Massif, Western Alps. In: SCHREYER, W. and STÖCKHERT, B. (eds): Special Issue: HP-metamorphism in nature and experiment. International lithosphere programme contribution 327. Lithos 41, 5–24.

MONIÉ, P. (1984): Etude par la méthode $^{39}Ar/^{40}Ar$ de la redistribution de l'argon dans les minéraux des socles anciens repris par l'orogenèse Alpine. Application à la géochronologie des Massif de l'Argentera-Mercantour, du Mont-Rose et de la Grande Kabylie. Thèse Université de Montpellier, 206 pp.

MONIÉ, P. and CHOPIN, C. (1991): $^{40}Ar/^{39}Ar$ dating in coesite-bearing and associated units of the Dora Maira massif, Western Alps. Eur. J. Mineral., 3, 239–262.

PAQUETTE, J.-L., CHOPIN, C. and PEUCAT, J.-J. (1989): U–Pb zircon, Rb–Sr and Sm–Nd geochronology of high to very high pressure metaacidic rocks from the western Alps. Contrib. Mineral. Petrol., 101, 280–289.

RUBATTO, D., GEBAUER, D. and COMPAGNONI, R. (1997): Three subduction episodes in the Western Alps between uppermost Cretaceous and Upper Eocene. Abstract EUG, Strasbourg, France, 23–27th March.

SCAILLET, S., FÉRAUD, G., LAGABRIELLE, Y., BALLÈVRE, M. and RUFFET, G. (1990): $^{40}Ar/^{39}Ar$ laser-probe dating by step heating and spot fusion of phengites from the Dora Maira nappe of the western Alps, Italy. Geology, 18, 741–744.

SCAILLET, S., FÉRAUD, G., BALLÈVRE, M. and AMOURIC, M. (1992): Mg/Fe and [(Mg,Fe)Si–Al_2] compositional control on argon behaviour in high-pressure white micas: A $^{40}Ar/^{39}Ar$ continuous laser-probe study from the Dora-Maira nappe of the internal western

Alps, Italy. Geochim. Cosmochim. Acta, 56, 2851–2872.
SCHERTL, H.-P., SCHREYER, W. and CHOPIN, C. (1991): The pyrope-coesite rocks and their country-rocks at Parigi, Dora Maira Massif, Western Alps: detailed petrography, mineral chemistry and PT path. Contrib. Mineral. Petrol., 108, 1–21.
SPENCER, D. and GEBAUER, D. (1996): SHRIMP evidence for a Permian protolith age and a 44 Ma metamorphic age for the Himalayan eclogites (upper Kaghan, Pakistan): implications for the subduction of Tethys and the subdivision terminology of the NW Himalaya. 11th Himalayan-Karakoram-Tibet Workshop (Flagstaff, Arizona, USA), Abstract Volume, 147–150.
TILTON, G.R., SCHREYER, W. and SCHERTL, H.-P. (1991): Pb–Sr–Nd isotopic behaviour of deeply subducted crustal rocks from the Dora Maira massif, Western Alps, Italy II: what is the age of the ultrahigh-pressure metamorphism? Contrib. Mineral. Petrol., 108, 22–33.

O. Müntener, J. Hermann and V. Trommsdorff (Zürich):

Permian and Jurassic metamorphisms associated with magmatism, extension and exhumation of a crust-mantle section (Malenco, Alps).

Lower crustal metapelites and ultramafic mantle rocks are welded together by a Permian gabbro in the Malenco unit (eastern Central Alps). The gabbro intrusion caused granulite facies metamorphism (T = 750–820 °C, p ~ 1.0 GPa) in the surrounding rocks and partial melting in the metapelites. Granulite facies conditions in connection with penetrative stretching outlasted the intrusion and resulted in a pervasive flaserisation and partly recrystallisation of the gabbro.

A two stage metamorphic history, subsequent to granulite facies metamorphism, has been recognized in all rocks of the section. The first stage involved cooling to ~ 600 °C with only minor decompression to ~ 0.8 GPa; the second stage was associated with increasing hydration and strong decompression ending at near surface conditions. Ar–Ar dating of amphiboles formed during initial hydration resulted in Jurassic ages. In table 1, the mineral parageneses and approximate metamorphic conditions are summarized.

The presented data are interpreted as follows: The gabbro intruded in an overall extensional environment which was typical for the future Mediterranean area during the Permian. The flaserisation of the gabbro in granulite facies conditions indicates that extension outlasted the intrusion. This is supported by the moderate decompression from ~ 1.0 to ~ 0.8 GPa subsequent to the granulite facies metamorphism. The recrystallisation at this pressure and temperatures of about 600 °C indicate the establishment of a stable crust-mantle transition at about 30 km depth. This situation lasted over a period of about 50 million years until Jurassic rifting commenced. This rifting led to hydration and exhumation that is recorded in a retrograde metamorphic evolution of all rock types of the crust-mantle section. The section then was integrated in the passive continental margin of the Adria plate.

Tab. 1 Parageneses and p-T estimations in the different rock types of the crust-mantle section.

Event	Metamorphism	Gabbro	Pelitic granulites	Ultramafic rocks	p-T estimations
Gabbro intrusion (Permian)		cpx + opx + pl + spi + ol ± ilm	partial melting gabbro dikes	gabbro dikes	1250 °C 1.0–1.1 GPa
near isobaric cooling	Granulite facies	spi-cpx-opx corona	ky + gar + qz + pl + ilm ± bio	ol + opx + cpx + spi + Ti-parg	800 °C 1.0 GPa
		gra-cpx-opx corona	Ca increase in gar ilm –> rut	ol + opx + sp –> chl	600–650 °C 0.8–0.85 GPa
hydration and decompression (Jurassic)	Amphibolite facies	gra-parg corona	ky + pl –> para + czo ky + gar –> st + ctd	cpx + opx -> ol + tr opx–> ol + tc	600 °C 0.8–0.85 GPa 525 °C 0.4–0.6 GPa
	Green-schist facies	(gra)-bio-hbl corona px –> act, hbl		atg + di	450–500 °C 0.2–0.4 GPa
Oceanic metamorphism	low p-T	Rodingites di + epi + gro + ves + tit + parg		chry + liz ± cc ± br	150–300 °C 0–0.1 GPa

M. Pfiffner and V. Trommsdorff

Calc-silicate rocks, Cima di Gagnone, Central Alps: relics of high-pressure metamorphosed ophicarbonates.

Coarse- to fine-grained calc-silicate rocks occur as pockets and wedges in ultramafic lenses of the Cima di Gagnone suite, and as attached masses connecting them. They form part of an ophiolitic sequence (EVANS et al., 1981; PFIFFNER, 1996) that was affected by Eocene (45–40 Ma, BECKER, 1993; GEBAUER, 1996) high pressure metamorphism. The Cima di Gagnone suite further consists of layered peridotitic rocks, including garnet peridotite, and eclogitic mafic rocks that have been rodingitized and boudinaged within the peridotites. The mafic rocks have MORB characteristics with magmatic major and trace element trends indicating low-pressure fractionation (EVANS et al., 1981). The calc-silicate rocks and metarodingites are locally crosscutting the layering in the peridotites and despite of Alpine deformation still display pre-Alpine sedimentary or tectonic contacts. In one outcrop, a fragmented boudin of metarodingite has been found within the coarse-grained calc-silicate rocks.

Mineralogically these calc-silicate rocks are fairly monotonous with up to 80 vol.% coarse-grained diopside (up to 10 cm), minor scapolite (75 mol% meionite, 25 mol% marialite), secondary amphibole (formed after diopside) and oligoclase/andesine (formed after scapolite), quartz and minor sphene, occasionally with rutile cores. Diopside typically contains 3 mol% jadeite component. Furthermore, the fine-grained calc-silicate rocks are enriched in Na_2O and show pseudomorphs of diopside (still containing up to 10 mol% jadeite component) and plagioclase (82 mol% albite) after omphazite demonstrating a precursor high-pressure metamorphic event.

Bulk chemical data of all calc-silicate rocks are clearly distinct from those of the mafic rocks. These data are slightly variable but most fall perfectly on mixing lines between the coexisting peridotitic rocks and calcite marbles. The major elements have proportions similar to diopside, which is the dominant mineral. Characteristics of minor and trace elements are high Cr- (up to 1000 ppm) and Ni- (up to 600 ppm), but low Zr- (less than 20 ppm) and TiO_2-contents (0.05–0.1 wt%) with proportions similar to those in the ultramafic rocks.

On the basis of field occurrence and chemical characteristics, it is evident that the calc-silicate rocks are remnants of former ophicalcite rocks. They formed as either fracture fillings within, or sedimentary deposits on top of denudated ex-subcontinental mantle peridotites exposed on an ocean floor. This supports the conclusion of EVANS et al. (1981) that the Cima di Gagnone suite represents a former ophiolitic association. During Alpine collision this suite was subducted and metamorphosed at 750–800 °C and 2.5–3.0 GPa.

BECKER, H. (1993): Garnet peridotite and eclogite Sm–Nd mineral ages from the Lepontine dome (Swiss Alps): New evidence for Eocene high-pressure metamorphism in the Central Alps. Geology 21, 599–602.

EVANS, B.W., TROMMSDORFF, V. and GOLES, G.G. (1981): Geochemistry of High-Grade Eclogites and Metarodingites from the Central Alps. Contrib. Mineral. Petrol. 76, 301–311.

GEBAUER, D. (1996): A P-T-t Path for an (Ultra?-) High-Pressure Ultramafic/Mafic Rock Association and its Felsic Country-Rocks based on SHRIMP-Dating of Magmatic and Metamorphic Zircon Domains. Example: Alpe Arami (Central Swiss Alps). In: Earth Processes: Reading the Isotopic Code. Geophys. Monograph 95, 307–329.

PFIFFNER, M. (1996): High pressure mafic and ultramafic bodies associated with calcsilicate rocks – a former ocean floor sequence and its evolution in the northern Cima-Lunga unit, Central Alps. Mitt. Österr. Miner. Ges. 141, 173–174.

Ph. Hunziker (Fribourg):

Thermobarometric investigations on amphibolites of the Silvretta thrust-sheet: implications for a Variscan tectono-metamorphic history. (Poster)

The Upper Austroalpine Silvretta nappe comprises approximately 1600 km^2 of crystalline rocks of which about one third are metabasites (mainly eclogites, amphibolites, metagabbros and metadiorites). The protoliths of the eclogites and the amphibolites respectively are the oldest rocks of the basement nappe and were formed during Proterozoic time. Two metamorphic high pressure overprints of these rocks preceded the Variscan metamorphism. The Variscan deformation and metamorphism was a polyphase amphibolite facies event which led to the formation of a marked penetrative foliation which characterizes all the rocks of the Silvretta nappe.

A number of amphibolites of the locality of Vernelatal (Graubünden, Switzerland) were investigated in the course of a diploma work at the University of Fribourg. The aim of the study was to decipher the imprint of Variscan metamorphism on amphibolites on the basis of thermobarometric calculations. Microprobe analysis were therefore performed on amphibole-plagioclase pairs which are in physical contact. Whenever a zonation was observed, rim composition was acquired. The lack of accurate activity models for amphiboles complicate thermodynamic investiga-

tions. Empirical models used for P-T-estimations revealed peak conditions of 550°–600°, 5–7 kb. Analysis of chemical differences and zonation trends in different generations of amphiboles and epidotes are expected to show a decrease of metamorphic conditions.

M. Passeraub, L. Holzer, K. Kreissig, T. Wuest and J. Kramers (Bern):

Horizontal tectonics at > 2.7 Ga in the Kaapvaal Craton: the Rhenosterkoppies Greenstone belt (RGB). (Poster)

The Rhenosterkoppies Greenstone belt is situated on the northern edge of the Kaapvaal Craton in immediate contact to the Southern Marginal Zone. Both terranes are separated by the supraregional Hout River Shear Zone, that is believed to have formed during the Limpopo Orogeny at about 2.7 Ga. Detailed mapping of the RGB in a 1:50'000 scale show that the entire belt consists of stacked, individual layers, that horizontally could be traced over the entire belt. Six different layers of banded iron formation within this supracrustal succession could be distinguished and underline the economic potential of the RGB. Seismic data suggest a shallow structure of the RGB, which is embedded within tonalitic gneisses. Sheared granites and gneisses crop out in a tectonic window in the central, lower part. The overall metamorphic conditions are of amphibolite facies grade, syntectonocally retrogressed to greenshist facies conditions. A precursor granulite facies assemblage is indicated by relictic cpx. Foliations in the central part are roughly horizontal progressively steepening up to 80° in the northwestern arm, where a drastic change in lithologies occurs. A prominent mineral lineation direction, mainly defined by hbl, and widespread qtz rodding are very consistent, trending NE–SW. Retrogressive, aligned titanite revealed an age of 2729 Ma, which coincides with ages of syn D1 pegmatites. It is concluded, that the stacked succession of the RGB is caused by tectonical thrusting. The northern, steeply N dipping portion of the belt is interpretet as a possible ramp, and the horizontal portion as a flat, the displacement of which is greater than 20 km. The tectonics of the RGB is older than the peak metamorphic condition in the SMZ, which occurred at 2690 Ma. The subsequent exhumation and overthrusting of the granulite facies SMZ onto the Kaapvaal Craton, that lasted till 2.6 Ga., was a non penetrative event with respect to the RGB. The thrusting found here at 2.73 Ga was thus part of a separate Archean orogenic event.

M. Schmocker (Fribourg):

Mikrostrukturelle und petrologische Untersuchungen an Hellglimmern und Granaten des Augengneises Typ Mönchalp, Silvrettakristallin (Graubünden).

Microsructural and petrologic investigations of micas and garnets of the Mönchalp augen-gneiss, Silvretta crystalline basement (Graubünden). (Poster)

In der austroalpinen Silvrettadecke lassen sich in den "Älteren Orthogneisen", zu denen gabbroide, dioritische, granodioritische sowie granitische Intrusiva gehören, seltene Hochdruckrelikte beobachten (MAGGETTI, 1986). Es handelt sich hierbei um Rutil- und Zoisitrelikte in Metadioriten und Metatonaliten, Granatkoronas um Pyroxen und Plagioklas in Metagabbros sowie Granatkoronas um Biotit herum im Augengneis Typ Mönchalp des Val Barlas-ch. Die zeitliche Einstufung dieses Hochdruckereignisses ist zurzeit noch unklar: Entweder sind die beobachteten Anzeichen das Resultat einer präkambrischen, eklogitfaziellen Hochdruckbelastung oder aber einer zweiten, späteren Überprägung unter derartigen Bedingungen (POLLER, 1994). Hauptsächliches Ziel dieser Arbeit ist, weitere Hinweise auf eine Hochdruckmetamorphose im Augengneis Typ Mönchalp zu erhalten. Die mikroskopische Durchsicht von rund 240 Proben zeigte, dass typische Hochdruckminerale fehlen, dass aber Granatkoronas um Biotit verhältnismässig häufig auftreten (u.a. in der Typlokalität Pischa/Mönchalp). Selten lassen sich bis zu 0,1 mm grosse, idiomorphe Granate beobachten, die nur im Kornkontakt mit Kalifeldspat und Plagioklas stehen und die mindestens zwei Wachstumsphasen aufweisen, die chemisch leicht unterschiedlich sind. Hochdruckfazielle, reliktische Mineralinklusionen wurden in keinem der beiden Granattypen gefunden.

Mit Hilfe mikrostruktureller sowie chemischer Argumente werden verschiedene Hellglimmergenerationen in Proben des Augengneises Typ Mönchalp der Typlokalität Pischa/Mönchalp unterschieden und mineralchemisch analysiert. Alle Proben zeigen eine ± stark ausgebildete, auf die variszische Orogenese zurückzuführende Schieferung, wobei der Grad der Rekristallisation stark variiert. So zeigen einige Proben fast ausschliesslich prädeformativ gebildete, mit ihren Längsachsen in die Schieferungsebene rotierte Hellglimmer ohne Rekristallisationserscheinungen, währenddem in anderen Proben überwiegend syndeformativ rekristallisierte Hellglimmer auftreten. Magmatisch gewachsene Hellglimmer lassen sich aufgrund mehrerer Kriterien von metamorphen

Hellglimmern unterscheiden, womit Aussagen über die Intrusionstiefe des granitischen Magmas möglich sind. Weiter wird untersucht, inwieweit die unterschiedlichen Glimmergenerationen während der variszischen Phase equilibriert worden sind. Speziell wird dabei auf eventuell vorhandene Zonierungen in den prädeformativ gebildeten Hellglimmern geachtet, da sie Hinweise auf eine frühere Hochdrucküberprägung liefern könnten.

MAGGETTI, M. (1986): Petrographische Kriterien zur Altersstellung des Hochdruckereignisses in der Silvrettamasse. Fortschr. Mineral. 64 (1), 103.

POLLER, U. (1994): Petrographie, Geochemie und Datierung der Augengneise Typ Mönchalp (Ältere Orthogneise) des Silvrettakristallins, Graubünden / Schweiz. Dissertation, Univ. Fribourg.

S.A. Sergeev and R.H. Steiger (Zürich):

Application of novel sub-grain scale analytical techniques in zircon U/Pb geochronology to enhance the history of the polymetamorphic augen gneiss (Central Swiss Alps). (Poster)

Insight into the history of polymetamorphic rock units which have survived a succession of overprinting events is of fundamental importance for geodynamic modelling. Precise age determination and the high resolution necessary for separating nearly simultaneous events can be achieved only by analysis of the resistant mineral chronometers (e.g. zircon). While geochronology of polymetamorphic units is notoriously difficult, the combination of microanalytical techniques involving high-precision isotope dilution methods permits age determination of sub-grain zircon systems formed during different stages of the rock history and offers insights beyond single-grain dating. Recently we have introduced new techniques which in combination with our ultra-clean laboratory facilities permit: 1) dating the accessory mineral grains coexisting with rock-forming minerals (SERGEEV et al., 1995) and 2) isolation and dating of genetically and chronologically independent mineral phases within single grains (STEIGER et al., 1993; SERGEEV et al., 1997).

At least one quarter of the pre-Mesozoic basement exposed in the Gotthard massif, Central Swiss Alps, is comprised of acidic augen gneiss (Streifen gneiss = SG), which traditionally was considered as a late-Caledonian porphyric intrusive, despite its structurally oldest position in the massif. The igneous nature of the SG is supported neither by our field and petrographical observations nor by its geochemical parameters. Inhomogeneity on a macroscopic scale as demonstrated by presence of large elongated layers of sedimentary quartzites, paragneiss and amphibolites cannot be interpreted as xenolithic inclusions but may represent tectonic wedges of overlying series. The occurrence of nebulitic domains within the SG, consisting of metasedimentary lithologies, is typical. Irregular distribution of quartz-feldspar augen in SG rock matrix argues for the porphyroblastic nature of the augen that originated during fluid infiltration through the SG precursor. The latter process is recorded in complete resetting of the Rb/Sr isotope system of the SG as advocated by whole-rock Rb/Sr analytical data (ARNOLD, 1970).

The SG zircon population consists mainly of elongated euhedral grains. Small isometric zircon grains of probably detrital origin are very subordinate (less than 1%). In the rock matrix elongated euhedral grains often show cores and a complex internal morphology. In feldspar augen, from which zircon grains were directly extracted, elongated grains typically exhibit regular zoning and lack visible cores. We analysed representative whole and abraded single zircon grains of distinct morphological types from different rock constituents as well as zircon fragments. Prior to introduction of our novel sample preparation technique by microtome, zircon fragments were mechanically cleaved from whole grains as morphological parts (e.g. crystal tips or visible cores). With the advent of the microtome (SERGEEV et al., 1997), we cut selected grains along the c-axis to obtain two mirror-image sections. One half-zircon is investigated by cathodoluminescence (CL) imaging and then by electron- and ion-microprobe (SHRIMP). On the basis of the CL images, the opposite half-grain is additionally sliced into recognized homogeneous crystal domains. The obtained domains were abraded and analyzed by highly precise isotope dilution (ID) techniques.

The ID results show that the zoned mantle of grains from the rock matrix yields a concordant U/Pb age of 442 Ma, whereas the zoned mantle of grains from augen – which we interpret as porphyroblasts – display concordant ages of 450 Ma. The zoned elongated core of the euhedral matrix grain yields the same concordant age of 450 Ma as the zircon mantle from grains in the feldspar porphyroblasts. Zircons captured in the feldspar augen terminated their growth 450 Ma ago, whereas zircons remaining in the matrix were later overgrown by a new phase 442 Ma ago. This suggests that porphyroblastesis preceded the recrystallization of the rock matrix by some 8 Ma. The upper intercepts of the regression lines obtained from discordant rounded cores indicate ages of ca. 0.7, 0.9 and 2.0 Ga for the precursors of the SG. Concordant ion-probe (SHRIMP) data confirm the

reality of the above protolith ages and in addition suggest the existence of a 500–520 Ma event and help to distinguish localization of different zircon phases wit hin complex zircon grains.

ARNOLD, A. (1970): On the history of the Gotthard massif (Central Alps, Switzerland). Eclogae geol. Helv. 63, 29–30.

SERGEEV, S.A., MEIER, M. and STEIGER, R.H. (1995): Improving the resolution of single-grain U/Pb dating by use of zircon extracted from feldspar: application to the Variscan magmatic cycle in the Central Alps. Earth Planet. Sci. Lett. 134, 37–51.

STEIGER, R.H., BICKEL, R.A. and MEIER, M. (1993): Conventional U–Pb dating of single fragments of zircon for petrogenetic studies of Phanerozoic granitoids. Earth Planet. Sci. Lett. 115, 197–209.

SERGEEV, S.A., KOMAROV, A.N., BICKEL, R.A. and STEIGER, R.H. (1997): A new microtome for cutting hard submillimeter-sized crystalline objects for promoting high-resolution instrumental microanalysis. Eur. J. Mineral., 9/2, 449–456.

A. Stucki (Zürich):

The high grade units of the Ivrea Zone in the Ossola Valley (Province Novara, Italy) *(see p. 157–161, this issue).*

GEOCHRONOLOGY AND GEOCHEMISTRY

J.D. Kramers (Bern):

Thoughts on continent growth and recycling based on comparisons of old and young orogens and reservoir modelling *(see p. 169–174 this issue).*

Th.F. Nägler and J.D. Kramers (Bern):

Nd isotopic evolution of the upper mantle: A forward modelling approach.

We present a dual approach to resolve the terrestrial evolution of the Sm–Nd system: a reviewed compilation of Precambrian Nd initials with reference to data from the oldest lunar rocks, and an independent forward modeling of the upper mantle development using a transport balance model, whereby present-day concentrations and Nd isotope ratios of upper mantle and crustal reservoirs are targeted (cf. NÄGLER and KRAMERS, 1997). The used transport balance model is identical to the published one used to reconcile data in the Th–U–Pb system (KRAMERS and TOLSTIKHIN, 1997). It is constrained by siderophile element (KRAMERS, 1997) and noble gas data and its reservoirs. Further, in a first order attempt it reconciled Re–Os data on Zimbabwean chromites, tracing the subcontinental lithospheric mantle evolution (NÄGLER et al., 1997). Successful models produce a very narrow range of ε_{Nd} development curves for the upper mantle. All these scenarios show very little recycling of continental crust into the upper mantle before 2–1.6 Ga ago.

The data as well as the model show a steady increase of the $\varepsilon_{Nd}[T]$ value of the upper mantle from 3 Ga on to a present day value of +10. In the Early Archean, a constant $\varepsilon_{Nd}[T]$ Nd value is seen. The model predicts that the upper mantle was not significantly different from Bulk Silicate Earth (BSE) in this early period. The data, however are generally one ε_{Nd} unit above CHUR. Lunar rocks also show this offset and, in particular, appear to indicate its existence since 4.5 Ga ago. This implies that the initial BSE and Moon are apparently slightly different from the conventional initial CHUR. Possible explanations for this apparent offset are some uncertainty of the CHUR model, analytical artifacts and interlaboratory bias. Published deviations from the accepted CHUR values and the effects caused by different fractionation correction procedures are all in the same direction, and make an *apparent* offset of c. +1 ε_{Nd} unit of terrestrial and lunar data relative to CHUR plausible. Measurements defining the accepted CHUR values (JACOBSEN and WASSERBURG, 1980) were done using NdO^+ beams and normalizing against $^{146}Nd/^{142}Nd = 0.636151$ (s. WASSERBURG et al., 1981). Most work on Archean terrestrial samples as well as much of the more recent work on lunar samples was done using Nd^+ beams and normalizing against $^{146}Nd/^{144}Nd = 0.7219$ (HAMILTON et al., 1983). The accepted present day CHUR $^{143}Nd/^{144}Nd$ ratio for $^{146}Nd/^{144}Nd = 0.7219$ normalization is derived using a linear translation. Using an exponential law for fractionation correction, this value should be +0.17 ε units higher (i.e. 0.512647). In addition, typical Nd^+ mass spectrometer runs tend to be under-fractionated relative to $^{146}Nd/^{144}Nd = 0.7219$ by 0.1–0.2% per mass unit. Using liner fractionation correction, a positive bias of between 0.2 and 0.4 ε units relative to the accepted CHUR system results.

Applying an apparent BSE evolution with an initial at one ε_{Nd} unit above the CHUR model brings terrestrial modeling of the upper mantle and data into good alignment.

A 3rd order polynomial fit to ε_{Nd} evolution curves generated by the model for the depleted upper mantle is given as a new reference for Nd model age calculations, via the relation:

$$\varepsilon_{Nd}[T]_{sample} = 0.164\,T^3 - 0.566\,T^2 - 2.79\,T + 10.4$$

HAMILTON, P.J., O'NIONS, R.K., BRIDGWATER, D. and NUTMAN, A. (1983): Sm–Nd studies of Archean metasediments and metavolcanics from West

Greenland and their implications for earth's early history. Earth Planet. Sci. Lett., 62, 263–272.
JACOBSEN, S.B. and WASSERBURG, G.J. (1980): Sm–Nd isotopic evolution of chondrites. Earth Planet. Sci. Lett., 50, 139–155.
KRAMERS, J.D. and TOLSTIKHIN, I.N. (1997): Two terrestrial lead isotope paradoxes, forward transport, modelling, core formation and the history of the continental crust. Chem. Geol., 139, 75–110.
KRAMERS, J.D. (1998): Reconciling siderophile element data in the Earth and Moon, W isotopes and the upper lunar age limit in a simple model of homogeneous accretion. Chem. Geol., in press.
NÄGLER, TH.F. and KRAMERS, D.J. (1998): Nd Isotopic Evolution of the Upper Mantle during the Precambrian: Models, data and the uncertainty of both. Precambrian Res., in press.
NÄGLER, TH.F., KRAMERS, J.D., KAMBER, B.S., FREI, R. and PRENDERGAST, M.D.A. (1997): Growth of subcontinental lithospheric mantle beneath Zimbabwe started at ≥ 3.8 Ga: A Re–Os study on chromites. Geology, 25, 983–986.
WASSERBURG, G.J., JACOBSEN, S.B., DEPAOLO, D.J., MCCULLOCH, M.T. and WEN, T. (1981): Precise determination of Sm/Nd ratios, Sm and Nd isotopic abundances in standard solutions. Geochim. Cosmochim., Acta 45, 2311–2323.

Urs Schaltegger (Zürich):

Dating Variscan granulites: Complex evolution – complex analytical toolbox (TIMS, SHRIMP, LAM-ICP-MS, CL, SEM).

This paper presents age determinations from granulites of the central Vosges mountains (France) that were formed during the Variscan orogeny. Granulites play a key role in the understanding of the Variscan belt, because they often represent the only information we have on the high-grade (and possibly prograde) part of orogeny.

Zircons of three granulite-facies rocks of igneous and sedimentary origin were dated by ionprobe (SHRIMP II at ANU, Canberra), conventional U–Pb and LAM-ICP-MS methods: $^{206}Pb/^{238}U$ SHRIMP ages of 335.4 ± 3.6, 334.9 ± 4.0 and 336.7 ± 3.5 Ma (95% c.l.) agree with a conventional U–Pb age of 335.4 ± 0.6 Ma (95% c.l.) for four single grains of one sample and date the age of granulite-facies metamorphism. The zircons display different morphologies as well as complex internal structures visible by cathodoluminescence, attributed either to subsolidus or melt growth. The different growth stages differ in their trace and rare earth element contents. SHRIMP spot ages from zircons with different morphologies (rounded anhedral vs prismatic euhedral) and from different types of growth zoning (sector domains, domains with "fir-tree" zoning, planar oscillatory zones) do not significantly differ, pointing to rapid growth under changing physico-chemical conditions. Trace and RE element concentrations and preliminary LAM-ICP-MS ages were determined by D. Günther using the Excimer laser (ArF, 193 nm) of the Institute for Isotope Geology and Mineral Resources at ETH Zürich (GÜNTHER, 1997) and agree with conventional and ionprobe data. This laser system has a better ablation behavior for zircon and is considered as a major improvement compared to Nd-YAG laser equipments.

The granulites are thus younger than volcanic and crosscutting magmatic rocks in lowest-grade metamorphic sedimentary basins bordering the central zone of the Vosges in the north and the south within a few tens of kilometers (SCHALTEGGER et al., 1996). It is suggested that the granulites were buried and exhumed rapidly during intracontinental transpressive shearing (SCHULMANN et al., 1997) During exhumation the granulites were rehydrated in amphibolite facies, and recrystallized or remelted at 328 Ma (U–Pb zircon). Monazites in recrystallized granulites kept their age from the peak of high-grade metamorphism (335.8 ± 0.6 Ma; $^{207}Pb/^{235}U$ age), while zircon ages were completely reset to 328 Ma. The case study demonstrates that U–Pb data from complex deep crustal domains can only be properly interpreted with detailed knowledge of the chemical and mineralogical properties of analyzed materials. A variety of imaging and dating methods is needed to fulfill this requirement.

Acknowledgements: These results are derived from ongoing collaboration with D. Günther (Zürich), J.C. Maurin (Strasbourg) and K. Schulmann (Prague), who are kindly acknowledged.

GÜNTHER, D., FRISCHKNECHT, R., HEINRICH, C.A. and KAHLERT, H.J. (1997): Capabilities of an ArF 193 nm Excimer laser for LAM-ICP-MS micro analysis of geological materials. J. Anal. Atom. Spectrom., 12, 939–944.
SCHALTEGGER, U., SCHNEIDER, J.L., MAURIN, J.C. and CORFU, F. (1996): Precise U–Pb chronometry of 345–340 Ma old magmatism related to syn-convergence extension in the Southern Vosges (central Variscan Belt). Earth. Planet. Sci. Lett. 144, 403–419.
SCHULMANN, K., SCHALTEGGER, U. and MAURIN, J.C. (1997): The Variscan Vosges massif: an example for extremely oblique transpression? Continental Transpressional and Transtensional Tectonics, March 5./6. 3. 1997, London.

B.S. Singer, Y. Vincze, W. Hildreth and T. Ton That (Genève, Menlo Park):

$^{40}Ar/^{39}Ar$ dating of latest Pleistocene lavas at Laguna del Maule, Chile: implications for the last glaciation of the Southern Andes.

$^{40}Ar/^{39}Ar$ incremental heating experiments were performed on 10 whole-rock samples from

Sample	Age spectrum	$^{39}Ar^{a}$ %	Isochron age(ka)[b]	$^{40}Ar/^{36}Ar$ intercept	Comments
Non-glaciated lavas					
Crater Bobadilla basalt	discordant	84	19.4 ± 7.4[c]		insufficient spread for isochron, use plateau age
Cerro Barrancas rhyolite	saddle	86	20.7 ± 0.6	295.6 ± 0.7	slight xenocrystic contamination?
West coast andesite	lower ages at low T	73	21.9 ± 3.4	298.8 ± 4.3	Ar loss; low T alteration?
Esperjos rhyolite	flat	100	23.3 ± 0.3	293.5 ± 0.8	very precise analysis
Crater Negro basalt	strongly discordant	64	239 ± 22[c]		very low % radiogenic Ar; negative isochron age
Glaciated lavas					
Lakeshore andesite	saddle	60	27.4 ± 1.7	239.8 ± 0.5	slight xenocrystic contamination?
El Candado basalt	flat	100	70.1 ± 3.0	293.8 ± 0.5	low and high T steps yield slightly lower ages
Domo del Maule	lower ages at low T	56	108.5 ± 13.7	296.3 ± 0.8	inherited argon? plus argon loss at low T?

[a] percent of gas contained in the plateau. [b] errors are at 1σ. [c] plateau age.

basaltic to rhyolitic lava flows erupted at 2150 m elevation in the Chilean Andes at 36 °S latitude in the vicinity of Laguna del Maule. This region of the Andes is currently devoid of large mountain glaciers, but was repeatedly glaciated during the Pleistocene (SINGER et al., 1997; HILDRETH et al., 1984). Eight lava samples that satisfy criteria of yielding age plateaus of more than three consecutive increments comprising > 50% of gas released are discussed here. The Domo del Maule rhyolite, El Candado basalt, and Lakeshore andesite lava flows are either deeply eroded or glacially striated. Younger lava flows that maintain pristine constructional morphologies and were neither eroded nor striated by glaciers include: Espejos rhyolite, Crater Bobadilla basalt, West Coast andesite, and Cerro Barrancas basalt. The table below summarizes the $^{40}Ar/^{39}Ar$ results and draws attention to details that influence how we have interpreted the age information.

Isochrons calculated from the plateau steps yielded ratios for the $^{40}Ar/^{36}Ar$ intercept that do not differ by more than 1% from the atmospheric value of 295.5. The Crater Negro basalt gave a strongly discordant age spectrum whose plateau age of > 150 ka is impossibly large given its unglaciated morphology; most steps contained < 1% radiogenic argon, thus we suspect that argon defining its plateau is largely inherited and does not reflect the age since eruption. Despite different bulk composition and mineralogy, and strong contrasts among their release spectra, samples from three unglaciated lava flows yielded isochron ages between 23 and 21 ka. The youngest of the three pre-glacial lavas gave an isochron age of 27 ka. The atmospheric $^{40}Ar/^{36}Ar$ intercepts of the isochrons indicate that excess argon is not present in quantities sufficient to give erroneous ages exceeding eruptive ages. Inherited argon residing in undegassed xenocrysts may have contributed to the older apparent ages in samples that gave saddle shaped spectra, but it is difficult to envision a contamination scenario that would lead to similar isochron ages from the three separate post-glacial lavas. Although we regard the likelihood of contamination with inherited argon as remote, investigation using a laser probe on biotite and feldspar separates are planned to further address this possibility.

If the isochrons are interpreted to reflect the time elapsed since eruption of these lavas, our results suggest that glaciers covered this area after 27 ka, but had receded before 23 ka. Lack of ice after 23 ka conflicts with estimates for the last glacial maximum (LGM) of 20 ka based on the global marine oxygen-isotope record (see discussion in GILLESPIE and MOLNAR, 1995), and with evidence from Lago Llanquihue moraines (41°S) which suggests that the LGM of the conterminous Patagonian icecap occurred at 21 ka, but also that a major re-advance of ice occurred at 14 ka (RABASSA and CLAPPERTON, 1990; ANDERSON et al., 1995). If our ages are correct, it may be that the icecap covering the Laguna del Maule region at 36 °S was separated from the Patagonian icecap and that its expansion and recession was influ-

enced by factors other than those affecting the larger more southerly Patagonia icecap.

ANDERSEN, B.G., DENTON, G.H., HEUSSER, C.J., LOWELL, T.V., MORENO, P.I., HAUSER, A., HEUSSER, L.E., SCHLÜCHTER, C. and MARCHANTS, D.R. (1995): Climate vegetation and glacier fluctuation in Chile, between 40° 30' and 42° 30' latitude – A short review of preliminary results. Quaternary International, 28, 199–201.

GILLESPIE, A. and MOLNAR, P. (1995): Asynchronous maximum advances of mountain and continental glaciers. Rev. Geophysics, 33, 311–364.

HILDRETH, W., GRUNDER, A.L. and DRAKE, R.E. (1984): The Loma Seca tuff and the Calabozos caldera: a major ash-flow and caldera complex in the southern Andes of central Chile. GSA Bull., 95, 45–54.

RABASSA, J. and CLAPPERTON, C.M. (1990): Quaternary glaciations of the southern Andes. Quaternary Science Reviews, 9, 153–174.

SINGER, B.S., THOMPSON, R.A., DUNGAN, M.A., FEELEY, T.C., NELSON, S.T., PICKENS, J.C., BROWN, L.L., WULFF, A.W., DAVIDSON, J.P. and METZGER, J. (1997): Volcanism and erosion during the past 930 k.y. at the Tatara-San Pedro complex, Chilean Andes. GSA Bull., 109, 127–142.

L. Holzer, I.M. Villa and J.D. Kramers (Bern):

Is old always slow?

The duration of Archean and Proterozoic orogens is difficult to unravel because of the generally polymetamorphic history preserved in old cristalline basements. With conventional geochronology (eg. U–Pb dating of zircon) complex and long lasting geological histories have been documented for most of these cristalline basements. This led to the conclusion that the evolution of old orogens was slow (several 100 Ma). We present data from the polymetamorphic Limpopo Central Zone (CZ) in Southern Africa, which confirm our previous observations in the Northern marginal zone and show that high grade metamorphic assemblages pertain to distinct events, therefore implying that each of these events lasted a much shorter time span than previously believed.

In recent studies the age of the various discrete (ductile) deformational phases in the CZ could be approximatively determined by means of crosscutting relationships with intrusive bodies of known age (KRÖNER et al., 1997; HOFMANN et al., 1997; HOLZER et al., 1997): 3290 > D1 > 3190 Ma, 2650 Ma > D2 > 2600 Ma, 2570 Ma > D3 > 2050 Ma, D4 = 2050–2000 Ma. However with conventional methods it was not possible to determine the metamorphic character (like peak conditions and PT evolution) of the distinct events. For this reason we applied Pb stepwise leaching to silicates like garnet, orthopyroxene and sillimanite from well defined metamorphic parageneses and reaction textures. A major target was to identify the age of peak assemblages from the various high grade events and the associated PT-evolution.

Pelitic assemblages of sillimanite coexisting with either garnet or orthopyroxene (rocks with high Mg/Fe) characterise high pressure granulite metamorphism. Subsequently these minerals react to form cordierite during decompression, indicating a clockwise PT-evolution. Pb stepleach ages between 2080 to 2030 Ma for garnet and enstatite from these assemblages determine the time of peak metamorphism during high pressure granulite facies metamorphism (M4). The timing of the retrograde path, associated with the exhumation of the CZ granulites, is documented by a large variety of U–Pb (monazite, titanite, apatite, rutile), Rb–Sr (biotite, muscovite) and Ar–Ar ages (hornblende, biotite). These data indicate a rapid uplift to mid crustal levels within ca. 50 Ma after peak metamorphism. The tectonic relationships of this event have been outlined by KAMBER et al., 1996; HOLZER et al., 1995 and 1997 and can by summarised as a dextral strike slip orogeny, during which the final juxtaposition of the Kaapvaal and Zimbabwe cratons took place.

An earlier period of granulite metamorphism could be identified by stepleaching of relic assemblages in metapelite. Rectangular aggregates of sillimanite, with minor interstitial cordierite, garnet and rutile are interpreted as pseudomorphs after andalusite (with Fe–Mg inclusions). This assemblage thus documents heating at low pressures. The Pb leach spectra of sillimanite and garnet give an age of 2521 ± 4 Ma, identical with U–Pb monazite ages also from metapelites. These data indicate the time of a previously unrecognised granulite event with anticlockwise PT-evolution in the CZ, probably associated with the above mentionned D3-deformational phase.

On the whole peak assemblages of two different granulite events in the Limpopo CZ could be dated and the associated PT-path is indicated by preserved reaction textures (M4: clockwise PT-loop between 2050–1950 Ma and M3 anticlockwise PT-loop at 2520 ± 20 Ma).

Even older, but distinct high grade events (M1 and M2) are documented by crosscutting relationships of deformed or migmatised gneisses which predate 3.2 and 2.6 Ga old intrusions. As for many other Archean and Proterozoic high grade terranes also for the Limpopo CZ a long lasting orogeny (> 1 Ga!) had been postulated, which can now be subdivided into at least four separate events. The Limpopo example raises the question whether slowness of tectono-metamorphic processes in old orogens is a myth, stemming from a

scarcity of accurately interpretable age data for the ancient gneiss terranes.

A. Plas and G.L. Früh-Green (Zürich):

Petrologic and stable isotope constraints on serpentinization and alteration of oceanic ultramafic rocks. (Poster)

Detailed petrologic and stable isotope investigations were performed on oceanic ultramafic rocks recovered during ODP legs in the Hess Deep Valley (Pacific Ocean, Leg 147), in the Tyrrhenian Sea (Legl07), and on the Iberia Abyssal Plain (Leg 149). The highly serpentinized sequence of dunites, harzburgites, troctolitic and gabbroic rocks recovered at Hess Deep (ODP Leg 147) represent a young shallow mantle section formed at the East Pacific Rise at a fast spreading ridge and show unusually high serpentinization temperatures. The pervasive secondary replacement is dominated by lizardite, brucite, chrysotile, taenite (a FeNi-alloy, documented for the first time in ocean floor serpentinites), antigorite, magnetite, tremolite, talc, chlorite, and iowaite. Static serpentinization formed a typical mesh-textured pseudomorphic replacement of olivine and occurred at temperatures of at least 400 °C. The presence of antigorite confirms the high temperature nature of serpentinization.

All serpentinites considered in this study show the following similarities: a high degree of secondary replacement; serpentine chemistry characterised by low Al and high Cl and B contents; strongly negative δD-Serpentine; and positive $\delta^{18}O$ serpentinizing fluid. The main differences are: serpentinization temperature; presence or absence of taenite, talc and antigorite; $\delta^{18}O$ serpentine; degree and type of deformation; and degree of alteration after serpentinization. Amphibole and talc can be produced at temperatures higher than 500 °C during early fluid-rock interaction. However, replacement of primary phases at this stage is limited and in contrast with the massive hydration caused by serpentinization. The role of serpentinization in the emplacement of ultramafic bodies may be active or passive, depending on the tectonic setting. Shearing of the serpentinite texture is not only indicative of diapirism, but may be caused by large-scale tectonic processes, particularly in rifted passive margins. The calculated negative δD_{fluid} values for all samples considered in this study are either an artifact of uncertainties in the presently available serpentine-water fractionation factors or reflect processes occurring during hydrothermal circulation and alteration.

These processes are: (a) production of methane and/or molecular hydrogen in hydrothermal fluids caused by reactions of serpentine formation, resulting in extremely D-depleted CH_4 and H_2; (b) phase separation, producing various degrees of D-depletion in brines; (c) pressure dependence on the hydrogen fractionation factors of minerals. Despite the large volumes of fluid required for serpentinization, local gradients in the hydrogen isotopic signatures of the serpentines suggest a lack of true open system conditions and indicate that the isotopic composition of the fluid was not externally buffered. Inferred serpentinization temperatures vary from 150 to higher than 400 °C. The extremely high T-values at Hess Deep reflect the tectonic setting (rapidly rifted, very young crust produced at a fast spreading ridge) and furnish new limits for the hydration of ultramafic rocks in oceanic environments. Although the presence of antigorite in oceanic samples is an indication of high temperature, its absence cannot be considered an indication of low serpentinization temperatures. Mantle sections eposed at the ocean floor are mostly highly serpentinized. As a consequence, through the formation of magnetite, these rocks may play an important role in the production of marine magnetic anomalies.

J. Hernandez (Lausanne):

Tracking the Mesozoic hot-spot(s?) in the eastern Pacific ocean: geology, mineralogy and geochemistry of remnants of the Caribbean oceanic plateau.

The Caribbean plate is composed of oceanic crust thickened by oceanic plateau mafic magmas. This plate was likely to have formed in the Pacific and migrated during the Late Cretaceous and Eocene in the oceanic realm dividing the North and South American plates. During the Late Cretaceous-Early Tertiary, the southern part of the Caribbean plateau collided with the northwestern margin of South America leading to obduction of oceanic plateau terranes, now exposed in Costa Rica, Colombia, Ecuador, Curaçao and Aruba. In contrast, the northern part moved eastwards into the gap between North and South America. Accreted terranes along est-west trending strike-slip faults gives exposures of the plateau in Cuba and Hispaniola (Dumisseau formation in Haiti, Duarte complex in Dominican Republic). The basalts and picrites exposed in some remnants of the plateau are Late Cretaceous in age (90–83 Ma) and considered as possibly related to the Galápagos hot-spot. However, recent work in

Western Mexico, Ecuador shows that some E-MORB basalts and picrites representing remnants of the Caribbean plate are Lower Cretaceous in age.

In spite of numerous studies on the Caribbean plate, a number of uncertainties remain concerning the isotopic signatures, mineralogical evolution and age of the tectonized E-MORB exposed in these areas. The purpose of this talk is to report new data, acquired by recent work in Lausanne and other places (see footnote), on the mineralogy, trace element and isotopic composition (Sr, Nd, Pb) of basic rocks (picrites, ankaramites and plutonic mafic rocks) in some selected exposures in Ecuador, Hispaniola and Costa Rica. A comparison with rocks exposed in other parts of the plate (e.g. Western Mexico) provides compositional and structural information on the different levels of the Carribean plateau.

Note: This work is part of a collective work undertaken in collaboration with researchers of Switzerland, France, Caribbean, Central and South America, especially H. Lapierre, B. Mercier de Lepinay, M. Tardy, R.C. Maury, D. Bosch, P. Monié, M. Polvé, E. Jaillard, P.O.B. Baumgartner and many others.

It is also indebted to the work thesis of V. Dupuis (Nice–Lausanne), O. Arias (Lausanne), C. Freydier (Grenoble), C. Reynaud (Lausanne), M. Bissainte (Paris–Lausanne).

V. Dupuis, J. Hernandez, H. Lapierre, B. Mercier de Lépinay, R. Maury, and M. Tardy (Lausanne, Grenoble, Valbonne, Brest, Chambéry):

Petrology and geochemistry of the oceanic plateau picrites of the Cretaceous Duarte Complex (Central Cordillera, Dominican Republic). (Poster)

The Duarte Complex is a MORB type tholeiitic belt which crops out in the Central Cordillera of the Dominican Republic. New fields data allow to recognize three parts in the Duarte Complex. The first, almost devoid of metamorphic features, is composed by basaltic flows and ribbon chert of Jurassic. The second unit consists of amphibolites and gneissic amphibolites derived from basaltic and doleritic flows, basaltic tuffs and intercalated cherts. The third unit which represent the most part of the Duarte Complex is a thick pile of picritic basalts, ankaramites and hydromagmatic breccias intercalated with minor tuffs. The mafic lavas are affected by a zeolite to a high grade greenschist facies. They are mainly composed by diopside to augite-diopside associated or not with rare serpentinized olivine and Mg-hastingsite in a actinolitic and chloritic groundmass. Ar–Ar ages of 86 ± 1.4 Ma of both late magmatic amphibole from a picrite and hornblende from an amphibolite are perfectly consistent with those of leg 15 E-MORBs drilled from the Caribbean oceanic plateau. The picritic basalts and ankaramites display slightly enriched REE spectras similar with those of the Dumisseau formation (Haiti). They are noticeably enriched in incompatible elements relative to the N-MORB. Their ε_{Nd}'s vary from +5.7 to +8,3 and fall within the range observed for the OIB. The Sr isotopic ratios of fresh picritic and ultramafic samples as well as those of their cpx and Mg hastingsite are consistent with an OIB affinity [$(^{87}Sr/^{86}Sr)i = 0.703233–0.703602$]. The Pb isotopic ratios which reflect the contribution of an HIMU-like enriched component [$(^{206}Pb/^{204}Pb)i = 18.966–19.537$] show that the picritic basalts and the ankaramites are isotopically similar to mafics lavas from previously described occurrences of the Caribbean-Colombian plateau and to few Galápagos hotspot's basalts. Thus the cretaceous picritic basalts and ankaramites of the Duarte Complex are a remnant of the Caribbean oceanic plateau originated from a larger Galápagos plum-type.

The picrites: The spreader area of Duarte Complex consists of a high grade greenschist facies thick pile of metapicrites and metaankaramites flows, ultramafic sills, fine-grain tuffs, hydromagmatic breccias and minor intercalated sediments, cross-cuted by unmetamorphosed dolerites and acid-rocks and intruded later by tonalites. The REE patterns normalized to the chondrite of the Cretaceous metapicrites and metaankaramite are enriched in LREE relative to the HREE due to the presence of residual garnet in the melt. This patterns are consistent with those of the E-MORB basalts of Gorgona island (Colombia), Dumisseau formation (Haiti) and the south Isabela island of the Galápagos archipelago (Ecuador).

The spiderdiagrams normalised to the N-MORB are enriched in Nb, Ta, Zr and Ti and are characteristic of an enriched source.

The Zr/Nb ratios vs Nb show that the source of the metapicrites and the ankaramites is a mixing between the N-MORB and OIB end-members. The ε_{Nd} isotopic ratios of the mafic rocks which range from +5.6 to +7 (with a value around +8.3) are similar with those of the Caribbean-Colombian plateau. The ε_{Sr} ratios are too high because of the hydrothermal alteration. The Pb isotopic ratios are homogeneous and reflect the contribution of an HIMU-like enriched component [$(^{206}Pb/^{204}Pb)i = 18.996$ to 19.537)] like the tholeiites of the Costa Rica and Gorgona. The picrites and the

ankaramite are remnants of the most primitiv and probably the deepest levels of the Cretaceous Caribbean-Colombian oceanic plateau.

The picrites and ankaramites of Duarte Complex are rich in MgO (9.65 to 19.1 wt%) and TiO_2 (1.5 to 2.48 wt%). The ankaramites are richer in $Na_2O + K_2O$ (3.8 to ~ 4 wt%) than the picrites. The ultramafic lavas of Duarte Complex are mainly composed by augite-diopside clinopyroxene associated or not with serpentinized olivine (~ 20% of normativ olivine for the ankaramites to 30–50% for the picrites) and Mg-Hastingsite in a actinolitic and chloritic groundmass. An Ar/Ar age on the Mg-Hastingsite gave 85.4 ± 1.7 Ma.

The unmetamorphosed ribbon chert and pillow basalts unit outcrops in the Janico-La Vega-Jarabacoa area. The El Aguacate formation was dated, on the basis of radiolarian fauna by MONTGOMERY et al. (1994) from 148 to 160 Ma. This Jurassic unit which consists of a thin pile of well preserved ribbon cherts interbedded with fresh pillow basalts is slightly thrusted by a serpentinized peridotite belt mainly composed by serpentinized pyroxene cumulates intruded by deformed diabase dykes. The Jurassic pillow basalts REE patterns are slightly depleted in LREE and display a MORB affinity. Their Pb isotopic ratios reflect the contribution of a depleted component (DMM or EM1). The diabases dykes REE patterns are depleted in LREE relative to the HREE $0{,}52 < (La/Yb)N < 0{,}59$ and show a typical N-MORB affinities.

F. Parat, Ch. Picard and D. Cluzel (Geneva, Grenoble, Noumea):

The Cretaceous West and East Coast basalts of new Caledonia: an obducted oceanic plateau. (Poster)

The Poya terrane is exposed along the eastern and western coasts of New Caledonia. This terrane consist of submarine basalts and dolerites associated with pelagic sediments, the age of which ranges from Campanian to Early Eocene. The rocks of the Poya terrane were metamorphosed successively to the greenschist and blueschist facies, and thrust upon the pre-Neogene rocks during the Late Eocene. The igneous components of the Poya terrane consist of basalts, dolerites and gabbros which exhibit P-MORB, N-MORB tholeiitic, alkaline and boninitic affinities. The P-MORB tholeiites predominate and are characterized by an enrichment in LREE ($0.86 < (La/Sm)N$ 1.16; $1.06 < (Ce/Yb)N < 1.36$) and LLE, and ε_{Nd} (T = 80 Ma) ratios ($+3 < \varepsilon_{Nd} < +5$) which fall in the range of OIB. These geochemical features indicates that these P-MORB rocks could be the remnants of an Oceanic Plateau. The N-MORB tholeiites have been found in two localities. They display flat REE patterns with a marked depletion in LREE ($0.45 < (La/Sm)N < 0.68$; $0.64 < (Ce/Yb)N < 0.99$). With respect to N-MORB, these rocks are enriched in LLE and slightly depleted in Nb. Their ε_{Nd} (T = 80 Ma) ratios (+7 to +8) are higher than those of the aforementioned P-MORB but lower than those of typical N-MORB. These features suggest that these N-MORB tholeiites developed in back-arc setting (BABB). The alkali basalts have only been locally found at Pinjen Peninsula, near Kone. They are enriched in LREE ($1.69 < (La/Sm)N < 3.80$; $4.36 < (Ce/Yb)N < 9.84$), and LLE. Their ε_{Nd} (T = 80 Ma) (+7 to +8) indicate that they could derive from the partial melting of a deep seated garnet mantle source. All the positive and rather high values of ε_{Nd} of these tholeiites preclude any contamination by the continental crust and infer the presence of two different mantle sources. P-MORB may result from the melting (> 15%) of a relatively deep, "enriched" asthenospheric source, that could be related to a thermal rise responsible for the Upper Cretaceous break-up of the east-Gondwana margin, and the opening of a marginal basin. Subsequent OIB, BABB and boninites may have erupted as seamounts upon the oceanic lithosphere.

ORE DEPOSITS

A. Audétat, Ch.A. Heinrich, D. Günther and R. Frischknecht (Zürich):

Fluid Evolution of the Sn-W-mineralized Mole Granite (Australia).

The Mole Granite is an Early Triassic, highly differentiated leucogranite, representing one of the youngest intrusions of the New England Batholith. The high-level, sill-like intrusion is only partially unroofed and contains several small roof pendants of Permian metasediments and metagranitoids. The exposed part of the intrusion covers an area of about 650 km^2 and is the host for numerous vein-type W- and Sn-deposits. The W-deposits are highly concentrated at the margins of the granite, whereas the Sn-deposits occur within the more deeply eroded parts of the intrusion as well as near its margins. Basemetal deposits and complex sheeted vein systems occur in the metasediments above the unexposed parts of the granite.

The metal zoning described above does not reflect a simple temperature gradient, but is the con-

sequence of progressive vein formation over the whole period of crystallisation and cooling. This can be demonstrated by fluid inclusion studies on selected quartz crystals from several ore deposits.

These quartz crystals contain several recognisable growth zones, some of which allowing a clear correlation between the formation of growth zones and stages of ore deposition. Careful fluid inclusion petrography on these samples allowed to reconstruct a detailed fluid history for different deposits and to determine the p/T-conditions for each mineral precipitated.

In order to reconstruct the *chemical* evolution of the fluid, inclusions from all stages were analysed by LAM-ICP-MS. Allowing the chemical analysis of *individual* fluid inclusions (see FRISCHKNECHT et al., p. 223 this volume), this technique is of critical importance for this kind of study. Only with a detailed knowledge of the fluid composition at various stages it will be possible to evaluate the ore-forming process(es) by thermodynamic modelling.

Insights into the very first stages of fluid evolution of the Mole Granite are given by inclusion assemblages in quartz phenocrysts and in quartz crystals from miarolithic cavities: coexisting melt-, vapour- and brine inclusions clearly demonstrate that the first exsolving fluid already was in the two-phase region. Further stages of fluid evolution are preserved in quartz crystals from vein-type ore deposits. At the Sn-mineralized Yankee Lode, several pulses of hot, magmatic fluid could be recognised, each associated with an increase in fluid pressure. Cassiterite and tourmaline deposition occurred at 380 °C and approximately 200 bar, just at the beginning of a mixing line with cooler, meteoric dominated groundwater. Similar pulses of magmatic fluid ingress, some of which associated with quartz corrosion, have been observed from other deposits.

In order to evaluate possible metal partitioning between coexisting vapour and brine, inclusions of both types have been analysed with LA-ICP-MS. The coexistence is proved by their occurrence within the same pseudosecondary planes and the occurrence of inclusions of compositions intermediate between the end members. Copper concentrations in vapour inclusions are more than 100 times higher than in coexisting brine inclusions. Selective element transport by the vapour may in part be responsible for the observed metal zoning at the regional scale and for the formation of extensive quartz-topaz greisens at the upper margins of the intrusion.

Ch. A. Heinrich, A. Audétat and Th. Ulrich (Zürich):

Towards a more quantitative model for magmatic-hydrothermal ore formation.

Porphyry-style and other hydrothermal vein and replacement deposits associated with shallow intrusions are the result of a sequence of processes that are ultimately controlled by global tectonics. Subduction of crustal rocks leads to the formation of hydrous, Cl and S-rich melts. During crystallization of the melts in upper-crustal magma chambers, fluids exsolve and are focussed upward through veins emanating from structurally-controlled apophyses, fractured volcanic necks or surface-venting diatremes. Fluid cooling, phase separation and reaction of magmatic-hydrothermal fluids with wall rocks and surface-derived fluids lead to the concentrated precipitation of trace-metals and the formation of ore deposits along the transport path. Metal ratios in ore bodies resulting from essentially similar processes vary widely, from porphyry-type deposits with variably high Cu, Au and Mo contents, to W and Sn-rich polymetallic deposits with variable concentrations of As, Cu, Au, Ag, Pb, Zn and many other trace elements. A crude correlation exists between metal ratios in the deposits and the composition of the associated magmas: Cu-Au-rich deposits are typically associated with oxidised (magnetite-series) and mafic to intermediate magmatic complexes, whereas Sn-W-As-rich deposits are characteristically related to reduced (ilmenite-series) and acid granitoids.

Absolute and relative concentrations of heavy metals in magmatic-hydrothermal ore deposits are the key to the economics of the extraction of essential raw materials, and the chemical and mineralogical composition of the ores directly controls the environmental impact of mining and beneficiation (amount of land use, energy consumption, toxic waste production). To understand the geological factors controlling selective metal enrichment in magmatic-hydrothermal systems in a more quantitative way, the following key questions must be addressed:

– How does the major-element composition of magmas control the partitioning of trace-elements from silicate melt and rock-forming minerals to the magmatic-hydrothermal fluid phase?

– How does fluid phase separation at high T and moderate P affect the distribution of trace metals and complexing ligands between coexisting hypersaline brines and lower-density vapour?

– What are the chemical reactions of wall-rock alteration and ore-mineral precipitation that will maximise the concentrations of valuable metals

(or minimise those of toxic waste elements) in a large ore body?

– Which are the hydrodynamic controls and thermal consequences of fluid phase separation, and of mixing magmatic fluids with meteoric waters that infiltrate from the hydrosphere?

Quantitative investigation of the complex magmatic-hydrothermal process is particularly dependent on improved techniques for characterising paleofluids (Micro-PIXE and LAM-ICPMS for trace-element analysis of individual fluid inclusions; FRISCHKNECHT et al., p. 217 this issue) and the development of new computer codes to model the physical and chemical interactions between fluids and fractured rocks (including new equations of state for complex NaCl–H_2O-dominated ore fluids; LIU et al., p. 190 this issue). Integrated field data from two case-study areas, the Mole Granite Sn–W–Mo–As–Cu–Pb–Zn district in New South Wales (AUDÉTAT, p. 211 this issue) and a porphyry Cu–Au-deposit in the Farallon Negro Complex in NW Argentina (Bajo de la Alumbrera, ULRICH, in prep.), will provide the geological framework for first applications of these new analytical and modelling approaches.

APPLIED MINERALOGY AND PETROLOGY

M. Chiaradia, B.L. Gulson and K. MacDonald (North Ryde, Sidney, Goulbourn, Genève):

Contamination of houses by workers occupationally exposed in a Pb–Zn–Cu mine and impact on blood lead concentrations in the families.

The objective of this investigation was to evaluate the pathway of leaded dust from a lead-zinc-copper mine to houses of employees, and the impact on blood lead concentrations (PbB) of children living in those dwellings. Mine employees' houses were located in the city of Goulburn (NSW, Australia) about 40 km from the (Woodlawn) mine, so that contamination through atmospheric transport of leaded dust from the mine to the dwellings was improbable.

High precision lead isotope and lead concentration data were obtained on venous blood and environmental samples (vacuum cleaner dust, interior dustfall accumulation, water, paint) for eight children of six employees (and the employees) from the lead-zinc-copper mine. These data were compared with results for 11 children from occupationally unexposed control families living in the same city. The median (range) concentrations of Pb in vacuum cleaner dust was 470 (21–1300) ppm. In the houses of the mine employees, vacuum cleaner dust contained varying higher proportions of mine lead than did airborne particulate matter measured as dustfall accumulated over a three month period. The median (range) concentrations of lead in soil were 30 (5–407) ppm and these showed no evidence of any mine lead (supporting the lack of atmospheric transport of lead from the mine). Lead in blood of the mine employees varied from 7 to 25 g/dl and was generally dominated by mine lead (> 60%). The mean (SD) PbB in the children of the mine employees was 5.7 (1.7) g/dl compared with 4.1 (1.4) lg/dl for the control children (P = 0.02). The PbB of all children was always < 10 g/dl, the Australian National Health and Medical Research Council goal for all Australians. Some of the control children had higher PbB than the children of mine employees, probably from exposure to leaded paint as six of the eight houses of the control children were > 50 years old. In five of the eight children of mine employees > 20% of PbB was from the lead mine. However, in the other three cases of children of mine employees, their PbB was from sources other than mine lead (paint, petrol, background sources).

Our investigation suggests that houses of employees from a lead mine can be contaminated by mine lead even if they are not situated in the same place as the mine. Delineation of the mine to house pathway indicates that lead is probably transported into the houses on the clothes, shoes, hair, skin and in some cases, motor vehicles of the workers. In one case, dust shaken from clothes of a mine employee contained 3000 ppm lead which was 100% mine lead. The variable contamination of the houses was not expected given the precautions taken by mine employees to minimise transportation of lead into their houses. Although five out of the eight children of mine employees had > 20% mine lead in their blood, in no case did the PbB of a child exceed the Australian National Health and Medical Research Council goal of 10 μg/dl. Some children in the control families had higher PbB than children of mine employees. In two cases, this was attributed to a pica habit for paint. The low PbB in the children of mine employees may reflect the relatively low solubility (bioavailability) of the mine dust in 0.1 M HCl (< 40%), behaviour – for example, limited mouthing activity – or diet.

F. Girod (Lausanne):

Weathering of granitic rocks in the Alps: preliminary results from orthogneiss associated with the Randa rockfall (Mattervalley, Wallis, Switzerland), (see p. 179–184, this issue).

Guscioni, N. (Fribourg):

Stabilisation de résidus industriels dans l'argile de Hochwald (All.) par liaison céramo-pyroplastique.

Stabilisation of industrial waste in clay of Hochwald/Germany by ceramic binding.

Le travail de doctorat présenté est le fruit d'une collaboration entre l'Institut de Minéralogie et de Pétrographie à Fribourg, la Hochwald Ton GmbH en Allemagne et le bureau d'ingénieur I.B.S.T.E. à Oberkulm en Suisse. L'objectif est d'établir la faisabilité d'une stabilisation ou d'une valorisation de deux résidus industriels dans la céramique produite avec l'argile de Hochwald (50 km au nord de Saarbrücken, Allemagne).

La méthodologie du travail est la suivante: A) caractérisation des 3 composants de base: le mélange argileux (HWT), le premier résidu (REST): une poussière de filtre d'une usine procédant à des fontes de métaux légers et non ferreux et le second résidu (CR): une boue galvanique riche en CrIII; B) étude du comportement thermique individuel de ces 3 composants; C) étude du comportement thermique de différents mélanges entre l'argile de Hochwald et chaque résidu industriel et évaluation des produits céramiques (tests de compression, tests de lixiviation standards, structure poreuse, retrait, gaz émis, etc.).

Voici une synthèse des propriétés des céramiques avec ajouts de résidus industriels. Les ajouts de résidus dans HWT induisent les néoformations de cuisson suivantes: -REST: hauyne, sulfates -Ca (Na) et anorthite; -CR: eskolaite, anorthite, apatite et sulfates-Ca. Les lixiviats (extraits par dilution standardisée à l'eau) des céramiques (1000 °C, 2 et 4% poids de REST et 2 et 10% poids de CR) sont très positifs, toutes les valeurs sont en dessous des limites légales (suisses) pour des déchets stabilisés, et en dessous des valeurs limites légales (suisses) pour des matériaux inertes à l'exception des céramiques avec ajouts de CR qui libèrent tout de même trop de CrIII (0.1 mg/l avec 2% poids d'ajout au lieu des 0.05 mg/l exigés: deux fois trop). Les valeurs positives des lixiviats jusqu'à 2% poids d'ajouts de résidus sont à modérer en tenant compte des émanations gazeuses mesurées par analyses chimiques des substances pures et des tessons après leurs différentes cuissons (très évidentes avec les substances pures): émanations de Cl, Na, K, S (+ traces de Cu, Zn, Pb et Br) avec REST et émanations de Na et S (+ traces de Cl et éventuellement Pb) avec CR. Des efflorescences liées au soufre sont observées sur certains tessons. Finalement, les résistances à la compression relatives à la céramique équivalente en température sans ajout montrent que: avec un ajout de REST de 2.2% poids (à 1000 °C) et 9% poids (à 1100 °C), une perte de 50% de résistance relative a lieu, cette même perte de résistance est atteinte avec un ajout de 10% poids de CR (à 1000 °C), par contre à plus haute température (1100 °C), les ajouts de CR augmentent la fonte donc les résistances.

En fonction des données ci-dessus, la poussière de filtre n'est pas un bon additif pour céramique (sels, gaz, résistances) tandis que la boue galvanique montre des résultats favorables à moins de 2% poids d'ajout (matériel inerte, CrIII stabilisé en eskolaite, pas de Cr dans les émanations, pas de CrVI dans les lixiviats).

M. Chiaradia, B.L. Gulson, M. James, C.W. Jameson and D. Johnson (North Ryde, Sydney, Research Triangle Park, Lidcombe, Genève):

Identification of secondary lead sources in the air of an urban environment. (Poster)

High precision lead isotope data have been measured from particulates deposited on filters from two suburbs of Sydney (NSW, Australia) and gasoline from two main brands during the period January 1991–May 1996 to evaluate the source of lead in air following the phasing out of leaded gasoline in Sydney in 1986 and a 25% reduction of lead in leaded gasoline in 1994. These measures have resulted in a 75% reduction of lead in Sydney air nowadays as compared to the period in which leaded gasoline was used. Despite these positive figures, our results indicate that gasoline still accounts for more than 90% of the lead in the atmosphere of this city. However, when compared with an earlier investigation carried out in the period 1979–1981, our data show that a background source with a $^{206}Pb/^{204}Pb$ isotopic ratio higher than petrol has become detectable. We have used a best fitting mathematical procedure to identify the isotopic ratio and percentage contribution of this source to the air. The values that we have obtained are ~18.2 and ~7% respectively for the $^{206}Pb/^{204}Pb$ ratio and the percentage contribution. This method has allowed us to make more plausible hypotheses on the origin of the secondary sources of lead in the air of Sydney and could also be used in the case of other urban centers. One possible background source in Sydney could be soil-derived. Our data also indicate that soils contributing to Sydney air lead burden would carry not only natural lead, but could be partially contaminated with gasoline. We suggest that this contamination could be either primary, i.e. happening before the suspension of soil particles in the atmo-

sphere, or occur by mixing with street dust in the air of the metropolitan area. Unpublished data from the EPA using multi-element chemistry implies a significant contribution of soil lead to air lead in Sydney.

Burning of wood during winter is considered to contribute negligibly to lead in air because of the origin of the timber and its seasonal impact. Likewise, a background source from coal-fired powerstations north of Sydney could contribute some lead to Sydney air but not as a continuous supply. It is possible that the background source measured in Sydney be the result of a mixing of different sources, including those above and/or others untested. The main requirement of our data is that lead from all these sources must be homogenised in the atmosphere and have rather long residence times to contribute in a constant way to the lead burden in Sydney air. Finally an alternative and attractive hypothesis, based on comparison of our results with existing data, is that the background source identified in Sydney air is the same as that identified by ROSMAN et al. (1994) in Antarctica and attributed by those authors to South American sources.

ROSMAN, K.J.R., CHISHOLM, W., BOUTRON, C.F., CANDELONE, J.-P. and PATERSON, C.C. (1994): Anhropogenic lead isotopes in Antarctica. Geophys. Res. Letters 21, 2669–2672.

Nadja Leber (Fribourg):

Optimierung keramischer Produkte durch Zugabe von Sekundärrohstoffen.

Optimized ceramic products by addition of secondary raw material. (Poster)

Die Abfallentsorgung stellt heute die Industrie und die Gesellschaft im allgemeinen vor ein sehr grosses Problem. Deshalb werden in letzter Zeit vermehrt Sekundärrohstoffe als Zusatz von Primärrohstoffen in verschiedensten industriellen Produktionsverfahren eingesetzt, um die Qualität der Endprodukte zu verbessern, Ressourcen zu sparen und die Umwelt so wenig wie möglich mit Deponien zu belasten. Das Ziel meiner im November 1996 begonnenen Diplomarbeit ist, durch Zugabe eines aluminiumreichen Sekundärrohstoffes einen Beitrag zur Ökologie zu leisten sowie die Wärmedämmung keramischer Produkte durch erhöhte Porosität zu verbessern.

Die Laborversuche werden mit zwei unterschiedlichen Mergeln durchgeführt, die in der Industrie zur Herstellung keramischer Produkte bereits eingesetzt werden. Der erste Mergeltyp wird aus den Schichten der Unteren Süsswassermolasse gewonnen, weist eine magere Zusammensetzung auf und enthält Quarz, Plagioklas, Kalifeldspat, Kalzit, Dolomit, Goethit und Tonmineralien (Hauptoxide in Gew.%: SiO_2 55.33, Al_2O_3 13.46, CaO 8.51, Fe_2O_{3tot} 4.67, K_2O 3.06, MgO 2.88). Der zweite Mergeltyp hingegen stammt aus unbekannter geologischer Formation, ist sehr fett und besteht aus Quarz, Goethit und Tonmineralien (Hauptoxide in Gew.%: SiO_2 56.79, Al_2O_3 20.56, Fe_2O_{3tot} 8.72). Der Sekundärrohstoff stammt aus einer schweizerischen Firma, die in der Metallveredelung tätig ist und die sich durch modernste Verfahren auf die Verarbeitung des Aluminiums konzentriert. Der bei der Eloxierung entstandene Abfallstoff ist sehr rein und besteht bis zu 96 Gew.% aus Aluminiumhydroxid. Die Mineralphase ist Gibbsit $Al(OH)_3$. Durch die Laborpresse wurden pro Mergeltyp 7 Mischungen mit folgenden Mengen an Sekundärrohstoff hergestellt (Angaben in Gew.%): 0.0%, 0.05%, 1.0%, 2.0%, 3.0%, 4.0%, 5.0%.

Erste Untersuchungen der physikalischen Eigenschaften der Proben ergaben, dass eine Erhöhung der Porosität nur schwer mit der steigenden Menge an Sekundärrohstoffzugabe in Verbindung gebracht werden kann, da die gemessenen Unterschiede der Porositäten der Proben sehr klein sind und im Bereich des Messfehlers liegen. Zu diesem Zeitpunkt können also noch zwei mögliche Schlüsse aus den Resultaten der Analysen gezogen werden: 1) die Zugabe an Aluminiumhydroxid verursacht keine Porosität; 2) die beigemischten Mengen an Aluminiumhydroxid sind nicht gross genug

Zurzeit stelle ich neue Mischungen mit Zugaben von 10.0%, 15.0% und 20.0% an Sekundärrohstoff her (Angaben in Gew.%). Erwähnenswert ist bestimmt noch die beobachtete und unerwartete Auswirkung der Zugabe an Aluminiumhydroxid auf die Farbe der Proben. Mit zunehmendem Anteil verändert sich die Farbe graduell von rot-orange zu gelb.

A. Mais (Fribourg):

Erste Ergebnisse naturwissenschaftlicher Untersuchungen an der neolithischen bis eisenzeitlichen Ware vom Castel Grande (Bellinzona, Tessin, Schweiz).

First results of petrographic examinations on Neolithic to Iron age stone ware from Castel Grande (Bellinzona, Tessin, Switzerland). (Poster)

Die Ausgrabungen am Castel Grande durch DONATI (1985) in Bellinzona bieten eine einzigartige Möglichkeit, die Entwicklung der Keramik in der frühen mitteleuropäischen Geschichte über einen Zeitraum von etwa 4000 Jahren zu beob-

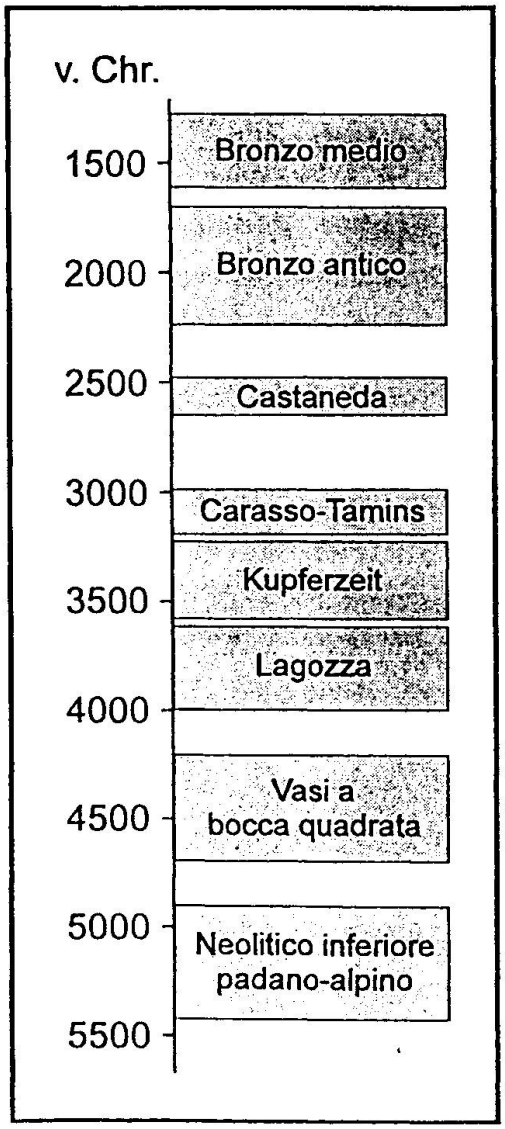

Zeittafel mit den verschiedenen Epochen der untersuchten Ware.

achten. Dies wurde durch eine detaillierte typologische Seriation der ausgegrabenen Ware von Carazzetti, R. ermöglicht, der eine komplette Abfolge der Kulturen vom frühen Neolithikum (etwa 5300 v. Chr.) bis zur mittleren Bronzezeit (etwa 1400 v. Chr.) nachweisen konnte (Abb. 1). In einer 1984 von SCHUBERT und MAGGETTI (1984) durchgeführten Studie wurden 13 Proben aus der jüngeren Bronze- bis Eisenzeit (etwa 1000 v. Chr.) mineralogisch-petrographisch und chemisch untersucht. In diesem, weitaus umfangreicheren Projekt sollen etwa 300 Scherben aus der vertikalen stratigraphischen Sequenz analysiert und mit denen anderer Fundorte verglichen werden.

Bis jetzt sind etwa 90 Proben der unterschiedlichen Epochen (Neolithikum bis mittlere Bronzezeit) genommen worden. Diese wurden mittels Polarisationsmikroskopie qualitativ und quantitativ untersucht. Aus der Beschaffenheit der Magerung lässt sich, zumindest bei der neolithischen bis kupferzeitlichen Ware, ein lokaler Ursprung vermuten. Die Mineral- und Gesteinsbruchstücke zeigen eine sehr gute Übereinstimmung mit den lokal auftretenden Gesteinen (v.a. Gneise, Glimmerschiefer und Amphibolite). Auch sind in der Magerung bislang keine Bestandteile identifiziert worden, die nicht in der Nähe des Ausgrabungsortes auftreten. Für die technologischen Untersuchung wurden Röntgendiffraktogramme erstellt und mittels Quecksilber-Druckporosimetrie die offene Porosität sowie die Porenradienverteilung bestimmt. Erste Ergebnisse deuten auf relativ niedrige Brenntemperaturen hin. Daneben wurde an den Scherben auch die Ritzhärte, die Farbe und die Farbverteilung untersucht.

DONATI, P. (1985): Bellinzona/TI, Castel Grande (Fundbericht), Jahrb. Schweiz. Ges. UsFrühg. 68, 210–215.
SCHUBERT, P., MAGGETTI, M. (1984): Mineralogisch-petrographische und chemische Analyse prähistorischer Keramik vom Castel Grande, Bellinzona TI. Bericht an den Archäologischen Dienst des Kantons Tessin, 45 pp., Berlin und Freiburg.

S. Wolf (Fribourg):

Technical investigation of bricks from St Urban (13th century Cistercian monastery, Lucerne, Switzerland): first results of the firing experiment. (Poster)

In the 13th century the Cistercian monks produced bricks of extraordinary size, design and quality at St Urban monastery. The majority of these building bricks are 45 · 34 · 11 centimetres, making them extremely unusual building materials. The brick sherds are temper-rich (up to 40 wt% temper), their colour ranges from a dark red to a brown-orange. The quality of the bricks varies from a soft porous to a hard and glassy matrix.

The research focuses on the technical aspects of the manufacture of these bricks. As it seems difficult to compare firing conditions in small electric kilns with production in the thirteenth century, a simple updraft kiln was built to imitate medieval brick making and firing. A firing experiment using this kiln was carried out in September 1997. During 10 days of firing temperature was registered at 18 positions in order to measure the temperature distribution at different levels in the ware chamber. We proved that differences in brick quality are mostly depending on the firing temperature and are due to the extreme temperature spread in the ware chamber. Maximum temperatures reached about 1300 °C near the flue and minimum temperatures of 600 °C at the front wall. Also the

temperature decreased from bottom above firing boxes to top of the ware chamber. We expected as well a temperature gradient within the bricks. X-ray diffraction patterns of the medieval building bricks show evidence that the temperature in the core was lower than in the rim of a single brick. With the experiment it was possible to measure the temperatures exactly: the temperature in the rim was about 60 °C higher than in the core.

In further investigations including water absorption, compressive strength, Hg-porosity and specific weight we will describe the technical and physical properties of the old and modern bricks. The comparison of the Cistercian bricks, their imitations and modern bricks may allow us a better assessment of brick production facilities and conditions in the 13th century.

A. Zanco (Fribourg):

Galloroman Terra Sigillata imitations from western Switzerland: 3 new reference groups. (Poster)

Three Galloroman TSI production sites dated from the 1st to the 3rd Century (A. D.) have been found in the Western part of Switzerland. Samples from these three sites, i.e. "Atelier du Stade" (Lausanne), "Atelier Faustus" (Yverdon) and "Atelier Faubourg NE" (Avenches), were studied in collaboration with the archaeologists of the University of Lausanne. Up to now 114 samples (51 from Lausanne, 32 from Yverdon and 31 from Avenches) have been analysed to characterise the production of each centre. The study was carried out on waste pieces of the workshops and fragments from kiln structures supposed to be of a local provenance. The first aim is the definition of three new reference groups and their comparison with stamped pottery, of unknown provenance. All the samples have been characterised following four steps:

1) Petrographic analysis, using a polarising microscope, on ceramic thin sections to describe structure, matrix, kind of tempers, their form, dimension, proportion and whether natural or added.

2) Chemical analysis (major and trace elements) using X-ray fluorescence.

3) Phase analysis, using X-ray diffraction, to identify phases present, whether primary, relict, firing or secondary minerals.

4) Hg-porosimetry to have information about micropores and their distribution.

The three productions have almost the same mineralogical composition consisting mainly of primary minerals like quartz, plagioclase and illite. Firing minerals are pyroxene, gehlenite and hematite. Wairakite and calcite are secondary. For most of the samples, firing temperatures have been estimated in the range of 850–950 °C. Some of the sherds were fired at temperatures higher than 950 °C and even attaining 1100 °C. Porosimetric data confirm such conclusions.

Geochemical data permitted establishing of three homogeneous groups among the sherds and to distinguish some dissident samples. These results should be employed as reference data for the attribution of about 90 stamped sherds of unknown origin.

BOCQUET, A. (1995): La production et la distribution des céramiques fines englobées et métallescentes dans le nord de la Gaule: approche minéralogique et géochimique (Louvain-La-Neuve), Ph.D, 214 pp.

HEIMANN, R.B. and MAGGETTI, M. (1981): Experiments on simulated burial of calcareous Terra Sigillata (mineralogical change). Preliminary results. In: HUGHES, M.J. (ed.): Scientific studies in ancient ceramics, 163–177.

JORNET, A. (1982): Analyse minéralogique et chimique de la céramique romaine suisse à enduit brillant. Institut de Minéralogie et de Pétrographie, Fribourg, Suisse Ph.D, 266 pp.

KÜPFER, T. and MAGGETTI, M. (1978): Die Terra Sigillata von La Péniche (Vidy/Lausanne). Schweiz. Mineral. Petrogr. Mitt., 58, 189–212 pp.

MAGGETTI, M. and KÜPFER, T. (1978): Composition of Terra Sigillata from La Péniche (Vidy/Lausanne, Switzerland). Archaeometry, 20, 2, 183–188 pp.

MAGGETTI, M. (1980): Recherches Minéralogiques, Chimiques et Technologiques sur la Terre Sigillée de l'atelier de la Péniche (Vidy/Lausanne). Cahiers d'Archéologie Romande, 20, Lausanne 4, 81–95 pp.

MAGGETTI, M. (1981): Composition of roman pottery from Lousonna (Switzerland). In: HUGHES, M.J. (ed.): Scientific studies in ancient ceramics , 33–49.

MAGGETTI, M. (1982): Phase Analysis and Its Significance for Technology and Origin. In: OLIN, J.S. and FRANKLIN, A.D. (eds): Archaeological Ceramics. Smithsonian Institution, 121–133.

PETERS, T. and IBERG, R. (1978): Mineralogical changes during firing of calcium-rich brick clays. Amer. Ceram. Soc. Bull. 57, 503–506.

PICON, M. (1984a): Traitement des données d'analyses. In: HACKENS, T. and SCHVOERER, M. (eds): Datation et caractérisation des céramiques anciennes, 379–399.

WHITBREAD, I.K. (1986): The Characterisation of Argillaceous Inclusions in Ceramics Thin Section. Archaeometry, 28, 1, 79–88.

ANALYTICAL METHODS

R. Frischknecht, D. Günther and Ch. A. Heinrich (Zürich):

Laser Ablation Microprobe – ICP-MS trace-element analysis of minerals and fluid inclusions.

Laser Ablation Microprobe-ICP-MS is one of the fastest growing analytical methods for high

spatial resolution analysis of trace elements in geological samples, and has great potential also for isotopic analysis. New types of lasers, the use of ultraviolet wavelengths and the development of new calibration strategies as well as highly sensitive ICP-mass spectrometers now allow routine in-situ elemental analysis in different sample types. These developments open new fields of geological applications in petrology, fluid and ore deposit studies and geochronology.

A Laser Ablation Microprobe – ICP-MS system using an excimer laser (193 nm, ArF) with a petrographic microscope in combination with an ELAN 6000 quadrupole ICP mass spectrometer will be described. High magnification optics of a converted petrographic microscope and a wide variety of laser parameters (e.g. adjustable pulse energies independent of the pit size, high repetition rates, and a homogenous laser energy distribution on the sample surface as well as a pulse to pulse stability of less than 1%) allow a much more controlled ablation process and a better interaction between sample and laser beam. The advantages of such a system for the ablation of solid materials will be shown with a trace element study on different zones of a natural calcite crystal, using a 20 mm pit size, whereby element concentrations down to ~100 ppb or less can be quantified.

Direct ablation of aqueous solutions has been introduced as a new calibration strategy for microanalysis of liquids as well as solids. This strategy forms the basis of LAM-ICP-MS analysis of major and trace element compositions of single fluid inclusions. Accuracy and precision of the calibration technique will be demonstrated on synthetic inclusions. Analytical reproducibility, the influence of daughter crystals on bulk microananlysis and actual geological variations are explored using samples with natural inclusions. Detailed study of the opening procedure of fluid inclusions can be monitored on line. First results indicate that detection limits as low as 1 ppm of heavy elements in a 30 mm inclusion may be reached. Precision is better than ± 20% for most elements with concentrations well above the detection limit.

Pb/U isotopic dating experiments will be presented for the SL13 zircon standard, which has been used for other zircon dating methods. The use of NIST 612 glass material as an external calibration standard demonstrates the greatly reduced matrix-dependence of ablation of the new 193 nm laser system. Preliminary results indicate that precisions around ± 2% in U/Pb ages may be reached, which is adequate at least for reconnaissance geochronology.

A.M. Lanfranco (Fribourg):

Characterisation of some micas by thermal treatments.

This study aims to analyse micas from Italian and Swiss Alps with several methods such as X-ray and HT-X-ray powder diffraction, TG, DTA and EGA concerning H_2O and CO_2. The crystallographic and mineralogical changes occurring in each heated sample are correlated with EMPA chemical determinations. X-ray powder diffraction data, collected before and after the thermal treatments are refined by Rietveld method (Siroquant program) to calculate the more probable unit cell.

According to thermal analyses (TG, DTA and EGA) certain temperature values have been set as critical conditions for the reactions in micas. Each transformation is reproduced in an oven and the resulting powders analysed. Using a LECO412 Multiphase Carbon Determinator the amount of total water loss from 25 to 1000 °C (100°/min rate of heating, oxygen atmosphere) was measured; the carbon content was also detected and its organic or inorganic nature determined.

Dehydroxylation in muscovite $2M_1$ starts at about 800 °C and causes 4–6% weight loss. The powders fired by LECO always showed b and c parameters increased, according to the literature data. Loss of interlayer cations should be responsible of 1% volume expansion because it can generate repulsion between TOT structure units. Thermal analyses of trioctahedral micas produced partially dehydroxylated biotite at 600–800 °C characterised by a total weight loss under 1%; the starting temperature for this reaction seems depending on Fe^{2+} content. By the LECO method about 4 wt% of water loss has been detected. Chemical variations in the octahedral sheets cause significant changes in the c parameter and the volume contraction was about 3%. The small quantity of organic carbon detected in both muscovite and biotite samples can be explained as contamination during the crystals grinding.

The phlogopite Mg rich sample from the Finero peridotite is the most stable sample showing a water loss peak at temperature higher than 1000 °C. In this mineral the amount of inorganic carbon approaches 1.75 wt%. The structural breakdown of micas has been promoted by heating the samples 2 days in oven at 1000 °C. The corresponding powder diffraction patterns contain either the peaks of new crystallised phases or the residual basal (001) reflections of micas.

P.G. Weidler, J. Luster, J. Schneider, A. Stahel, H. Stanjek and A.U. Gehrig (Zürich, München):

Die Rietveld Methode in der quantativen mineralogischen und chemischen Charakterisierung tropischer Böden.

Quantitative mineralogic and chemical characterization of tropical soils by the Rietveld method.

Für die qualitative und quantitative Charakterisierung der mineralischen Zusammensetzung von Böden ist die Röntgenbeugung (XRD) eine allgemeine Methode. Während die Beschreibung von mineralischen Einzelphasen mit dieser Methode keine Probleme bereitet, ist die quantitative Analyse von natürlichen Bodenproben mit mehreren mineralischen Phasen schwierig. Eine Möglichkeit, diese Quantifizierung durchzuführen, ist die Rietveld-Methode, die die Information des gesamten Diffraktogramms benutzt.

Trotz der massiven Überlappung der Braggreflexe konnten genaue und zuverlässige Gitterparameter für alle mineralischen Bestandteile gefunden werden. Aus diesen Daten konnten die Al–Fe-Substitutionen der Fe(hydr)oxide berechnet werden. Als Hauptkomponenten wurden Quarz und Kaolinit, als Nebenbestandteile Goethit, Hämatit und Anatas festgestellt. Aufgrund der chemischen Analyse der Bodenproben konnte die quantitative Analyse, die aus der Rietveld-Methode erhalten wurde, überprüft und somit der wechselseitige Einfluss der diversen Parameter der Verfeinerung und der verwendeten Wellenlängen (Cu $K_{\alpha 1/2}$, Cu$K_{\alpha 1}$, Mo $K_{\alpha 1}$, Co $K_{\alpha 1}$) untersucht werden. Zum Schluss wird die Anwendbarkeit dieser Methode auf Böden anderer Klimate diskutiert.

M. Engi and A. Cheburkin (Bern, Kiev):

Chemical dating of young monazites using the mini-XRF probe. (Poster)

Monazite holds promise for dating stages of high temperature deformation and/or high grade metamorphism because it appears to recrystallize readily when strained, and its Th–Pb and U–Pb systems remain closed up to rather high temperatures. During pophyroblast growth, monazite grains are frequently incorporated, notably in Al-silicates such as garnet. Such grains may thus evade recrystallization during subsequent deformational and metamorphic stages of evolution, while monazite in the matrix appear to recrystallize readily, especially in fluid-rich environments. For these reasons, monazite ages obtained from traditional mineral separates may not be interpretable, if they derive from rocks with a complex history, e.g. from polymetamorphic-polydeformed terrains. In such cases it is desirable to have methods to date individual monazite grains, either in situ in a thin section or after careful mineral separation from porphyroblasts or suitable structural domains. Monazite grains of > 100 Ma age contain ^{210}Pb (from ^{232}Th decay) to use the electron microprobe; for younger samples, the EMP fails due to its high detection limit (~ 100 ppm for Pb).

An improved version of the EMMA probe (CHEBURKIN et al., 1995) has been designed, built, and used successfully to date single grain monazites as young as < 15 Ma, even if the grain size was < 80 μm. The instrument used consists of a conventional 2 kW Mo X-ray tube, a focused LiF monochromator, a rotating stage holding the sample (mounted on 4 mm Prolene film) on a petrographic microscope, and a Si(Li) detector. For single grains as small as 50 mm the detection limits for U, Th and Pb are on the order of 10 ppm for analysis times 10 min., the time required to obtain ages to within 3–8% accuracy for each grain. While these uncertainties are substantial, compared to isotopic data, the defined spatial context and resolution lend confidence to their interpretation. Also, the data are simpler and much cheaper to obtain.

The method was tested on a set of monazite separates obtained from V. Köppel who generously provided a series of "leftovers" from his classical studies of Alpine monazite. Comparison of our results with those documented by KÖPPEL and GRÜNENFELDER (1975, 1978) and KÖPPEL et al. (1981) shows good overall agreement for most samples, but with definite deviations: Several of the samples contain younger, some of them older grains in with a majority of "normal" grains. Statistical analysis of populations (30–50 grains from single Alpine samples) commonly indicates bi- or trimodal age distributions. These can yield valuable information about pre-Tertiary evolutionary stages and/or indicate later resetting.

Since the new method is non-destructive, it may thus be used (a) for reliable (if somewhat imprecise) monazite dating and (b) to test whether and what monazite fractions should be dated more precisely by mass spectrometry or SHRIMP. Complex samples may contain sufficiently large groups of monazite grains to allow at least a preliminary interpretation of polymetamorphic evolution.

CHEBURKIN, A., FREI R. and SHOTYK, W. (1995): An energy-dispersive miniprobe analyzer (EMMA) for direct analysis of trace elements in single mineral grains. Chem. Geol. 135, 75–87.

KÖPPEL, V. and GRÜNENFELDER, M. (1975): Concordant U–Pb ages of monazite and xenotime from the Cen-

tral Alps and the timing of the high temperature Alpine metamorphism, a preliminary report. Schweiz. Mineral. Petrogr. Mitt. 55, 129–132.
KÖPPEL, V. and GRÜNENFELDER, M. (1978): The significance of monazite U–Pb ages; examples from the Lepontine area of the Swiss Alps. U.S. Geol. Survey Open File Rep. 78–701, 226–227.
KÖPPEL, V., GÜNTHERT, A. and GRÜNENFELDER, M. (1981): Patterns of U–Pb zircon and monazite ages in polymetamorphic units of the Swiss Central Alps. Schweiz. Mineral. Petrogr. Mitt. 61, 97–119.

R. Schönberg, Th.F. Nägler and R. Frei (Bern):

Recent improvements of Re–Os analytics in the Bernese Isotope Geology Lab. (Poster)

A number of improvements have been achieved for Re–Os analytics in our lab by changing the analytical hardware. Initially, Re and Os analyses were made using a "classical" setup (e.g. OsO_4 two times distilled in a glass apparatus after WALKER (1988); Re separation via two anion-exchange columns. Both, Re and Os, measured from Pt filaments). This setup turned out to be very time consuming, and minimizing blanks appeared to be a highly complicated task. Therefore the analytical setup was changed significantly: A time and cost efficient, simple and easy to assemble distillation line for efficient Os recovery (> 85%) from the digestion solution in a single step directly into HBr was developed. The distillation assembly is composed solely of off-the-shelf Teflon® material with the advantage of easily pluging in additional lines for the simultaneous distillation of a larger number of samples.

The main separation of Re from most of the rock matrix is now achieved by the solvent extraction described by WALKER (1988), because of its simplicity, speed and low blanks. This is followed by a cleaning step via anion exchange chromatography performed in microcolumns (80 µl resin). Re column chromatography is classically performed using HNO_3 of different molarities up to 8.8 M. However, strong nitric acid has the disadvantage of attacking the resin, which itself contains small amounts of Re and so may significantly increase the blank-levels. Furthermore, this effect brings in traces of organic matter into the Re fraction, which inhibits Re-oxide emission from the filament during mass spectrometric analyses. To overcome this problem, we tested an HCl–HBr milieu during anion exchange, which displayed ideal characteristics of high yields (> 90%) and low blanks (1–4 pg). Additionally the cleaned Re fraction is free of organic compounds, in contrast to the conventional HNO_3 column chemistry. This results in higher signals and therefore increased precision of the determination of Re isotopic composition. Re is now measured from $BaSO_4$ beds on Ta-filaments, which is less sensitive towards time consuming pre-analytical heating procedures as encountered with $Ba(NO_3)_2$ on Pt filaments. Furthermore, Re isotopic ratios remained constant over a wider range of temperatures, in contrast to what we observed during Re analyses from Pt filaments loaded with $Ba(NO_3)_2$ or $BaSO_4$. Our technique can be easily installed and ensures high quality, high yield and low blank (Os < 1 pg; Re < 20 pg) Re–Os separation for geochemical, cosmochemical and geochronological studies.

FREI, R., NÄGLER, T.F. and MEISEL, T. (1996): Efficient N-TIMS rhenium isotope measurements on outgassed tantalum filaments: Very low filament blanks determined by a "standard addition" approach. Int. J. Mass. Spectrom. Ion Proc., 153 (2–3), L7–L10.
NÄGLER, T.F. and FREI, R. (1997): "Plug in" Os distillation. Schweiz. Mineral. Petrogr. Mitt., 77, 123.
WALKER, R.J. (1988): Low-blank chemical separation of rhenium and osmium from gram quantities of silicate rock for measurement by resonance ionization mass spectrometry. Anal. Chem., 60, 1231–1234.